J. Fluid Mech. (1987), *vol.* 179, *pp.* 105–136
Printed in Great Britain

Growth and collapse of translating compound multiphase drops: analysis of fluid mechanics and heat transfer

By H. N. OĞUZ AND S. S. SADHAL
Department of Mechanical Engineering, University of Southern California, Los Angeles, CA 90089-1453, USA

(Received 14 May 1986 and in revised form 15 October 1986)

The time history is examined of the motion of a compound multiphase drop formed by a vapour bubble completely covered by its liquid phase in another immiscible liquid. The compound drop is growing or collapsing owing to change of phase while it is translating under buoyant forces. In the limit of large surface-tension forces the interfaces are spherical. An exact analytical solution for the fluid-mechanical part of the problem can be obtained. The heat-transfer treatment of the problem, however, requires numerical solution if we are to include convective terms along with time dependence. The drag component induced by radial velocity contributes to the total drag on the bubble in eccentric configuration. This drag force is towards the centre of the drop in the case of growth and has an effect of restoring concentricity. However, it is found that, in the case of growth, the compound drop, in general, cannot maintain its configuration of two non-intersecting eccentric spheres. On the other hand, in the case of collapse the bubble stays inside the drop if the collapse velocity is high enough. The complete analysis exhibits some interesting flow patterns relating to compound drops and bubbles. The time-dependent Nusselt number for a single bubble generally decreases with time but it may have a strong dependence on the compound-drop configuration, as well as the conductivities of the participating liquids. The radial convection opposes heat transfer but it has to compete with translatory convection, which is usually overwhelming in the case of growth.

1. Introduction

The study of the motion of spheres in fluids goes back as far as 1851 when Stokes first investigated the creeping motion of a solid sphere. Recently, there has been an interest in somewhat more complicated problems involving drops composed of two fluid spheres forming compound multiphase drops. We encounter such drops in processes such as direct-contact heat exchange, liquid-membrane technology and melting of ice particles. For the case of direct-contact heat exchange, one fluid is passed through another immiscible one at a different temperature. If a change of phase is allowed in the process one obtains compound drops involving three fluids.

In our earlier work (Sadhal & Oğuz 1985) we investigated the motion of compound drops purely from a fluid-mechanics point of view. Also an extensive review of the fluid mechanics of compound drops and bubbles has been recently given by Johnson & Sadhal (1985). In the present study we focus our attention on compound drops undergoing growth or collapse due to change of phase in immiscible liquids. In general the motion consists of radial growth or collapse as well as translation. The

growth/collapse introduces some interesting fluid-mechanical as well as mathematical aspects to the problem. The incorporation of change of phase requires the treatment of heat transfer along with the fluid mechanics in a coupled fashion. There is a great deal of interest in such drops in the field of direct-contact heat transfer because of the high efficiency achieved by eliminating the resistance between two phases. Sideman & Taitel (1964), Sideman & Hirsch (1965) and Isenberg & Sideman (1970) investigated the heat-transfer characteristics of evaporation and condensation of immiscible drops and bubbles from a heat-transfer point of view. Hayakawa & Shigeta (1974), Selecki & Gradon (1976), Tochitani, Mori & Komotori (1977*a*) and Tochitani *et al.* (1977*b*) have reported their work on the motion of two-phase droplets and on the fluid mechanics associated with it. In a recent investigation Lerner & Letan (1985) examined the condensation problem for cases when there is a thin condensate film. Jacobs & Major (1982) studied the collapse of compound drops taking into consideration the heat and mass transfer in the gas phase. Over the past few decades, there have been extensive investigations of two-fluid systems with change of phase. However much of this has been reviewed elsewhere (see e.g. Plesset & Prosperetti 1977; Prosperetti & Plesset 1978) and we shall not discuss it here. Our discussion is limited to three-fluid systems.

Most of the published works in the area are either experimental or concerned with only the heat-transfer aspects of the problem. The flow field is often approximated and little rigorous discussion about it can be found in the literature. It is the intent of this paper to provide fundamental understanding of the fluid mechanics coupled with the heat transfer for a class of two-phase droplets with change of phase. Although the configuration we are dealing with is somewhat limited, it is a starting point for more complex problems. The present work covers the configuration of two fluid droplets with one phase completely engulfing the other one. This configuration can be treated analytically with the use of the bipolar coordinate system. This coordinate system was invented by Jeffery (1912) and has been used by several authors for problems in fluid mechanics as well as in heat transfer. Among the well-known publications in this regard are the Stokes flow solutions given by O'Neill (1964), Goren & O'Neill (1971), Rushton & Davies (1973, 1978), Haber, Hetsroni & Solan (1973) and Meyyappan, Wilcox & Subramanian (1981). A numerical solution in the bipolar coordinate system for heat transfer and fluid mechanics of melting ice particles was given by Rasmussen, Levizzani & Pruppacher (1982). This was the case of a solid ice sphere coated with a water film. The outer surface of the film had a specified $\sin\theta$-type approximation for the tangential velocity. Since the change of phase for this case was only from solid to liquid, the radial velocity effects were absent.

In the next section we state the problem. For the fluid-mechanics part of the problem we consider creeping flow and derive its analytical solution. The heat transfer is coupled with the flow field and the energy equation is solved by finite-difference methods.

2. Analysis

2.1. *Statement of the problem*

We consider a liquid drop in an immiscible unbounded fluid at uniform temperature. Inside the drop there is a bubble growing or collapsing owing to the slow evaporation or condensation of the drop (see figure 1). The vapour bubble lies entirely inside the drop and its growth or collapse is slow. Driven by buoyant forces as well as the viscous forces the bubble in general translates relative to the drop along their line of centres.

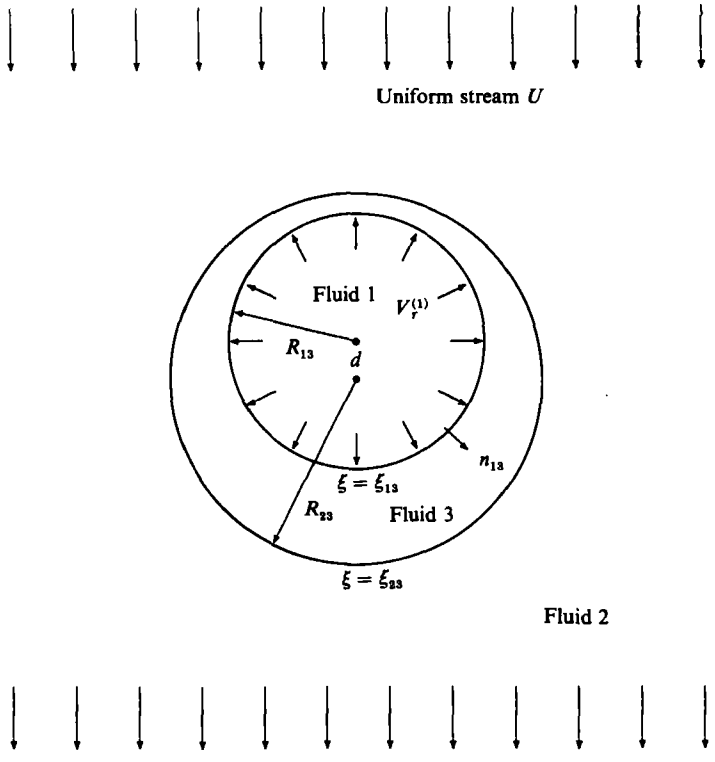

FIGURE 1. Schematic of the flow past a compound multiphase drop. The uniform stream has a velocity U relative to the outer spherical interface which is fixed in the coordinate system. The inner spherical interface moves at a velocity V relative to the outer interface. In addition the inner and the outer interfaces have a radial velocity $V_r^{(1)}$ and $V_r^{(2)}$ respectively.

We neglect the inertial terms and consider only Stokes flow. Since the bubble size changes slowly the problem is quasi-steady in terms of the fluid mechanics. Under the Stokes flow approximation we may consider the translational velocities as well as the flow field to be instantaneous, i.e. viscous diffusion does not participate in the time dependence. We choose to denote the velocity of the compound drop as U and the relative velocity of the bubble with respect to the drop as V. The translational velocities U and V are unknown and to be determined from the total force balance equations. We refer to the continuous phase as fluid 2, the drop as fluid 3 and the vapour bubble as fluid 1. We also assume that surface tension at both the interfaces is large enough to preserve the sphericity of the bubble and the drop. The interfaces are considered to be free of surfactants and the interfacial tension is therefore uniform.

The governing equations are as follows:

continuity:

$$\nabla \cdot \boldsymbol{u}_i = 0 \quad (i = 2, 3),$$

momentum:

$$\nabla p_i = \mu_i \nabla^2 \boldsymbol{u}_i \quad (i = 2, 3 \text{ (no sum)}),$$

where $i = 2, 3$ is used to denote the quantities in phases 2 and 3, respectively; p_i are the pressures, μ_i the viscosities and $\boldsymbol{u}_i$ the velocities. The boundary/interface conditions are:

(i) uniform stream U at infinity;
(ii) prescribed normal velocity $V_r^{(2)}$ at the outer interface;
(iii) continuity of tangential velocity at the outer interface;
(iv) continuity of shear stress at the outer interface;
(v) prescribed normal velocity $V_r^{(1)}$ at the inner interface;
(vi) zero shear stress at the inner interface.

Here the normal velocity $V_r^{(1)}$ is prescribed as an unknown constant which will be determined by the growth/collapse rate given by the heat-transfer rate. The normal velocity $V_r^{(2)}$ is related to $V_r^{(1)}$ by a volume constraint on phase 3.

For the heat-transfer part we consider the conduction/convection problem described below. Its solution will give the radial velocity $V_r^{(1)}$ which is necessary to fully define the flow field. We also note that the heat-transfer is coupled to the flow through the convective terms. The governing equations for this problem are as follows:

energy balance

$$(c_p \rho)_i \left(\frac{\partial T_i}{\partial t} + \boldsymbol{u}_i \cdot \boldsymbol{\nabla} T_i \right) = k_i \nabla^2 T_i \quad (i = 2, 3 \text{ (no sum)}),$$

where $(c_p \rho)_i$ is the heat capacity, T_i the temperature, k_i the conductivity of the respective fluids and t is the time.

The boundary/interface conditions are:

(i) uniform temperature T_∞ at infinity;
(ii) continuity of temperature at the outer interface;
(iii) continuity of heat flow at the outer interface;
(vi) constant temperature T_v at the inner interface (here T_v is the saturation or equilibrium temperature of the vapour (fluid 3)).

For brevity, these equations are written in mathematical notation only after the introduction of the stream functions for the velocity field.

We further make the assumption of small capillary number. At both the interfaces the surface tension dominates the viscous forces. This implies that, at any time, the bubble and the drop preserve their spherical shape. Therefore the size change of the bubble due to the phase change can only create a uniform normal velocity at the bubble–drop interface. An energy balance on the inner sphere surface gives the relation between the normal velocity $V_r^{(1)}$ and the temperature field as

$$\rho_1 L_3 V_r^{(1)} = \frac{1}{A} \int_A k_3 \boldsymbol{\nabla} T_3 \cdot \boldsymbol{n}_{13} \, \mathrm{d}A, \tag{1}$$

where A is the bubble surface area, ρ_1 is the density of the bubble, L_3 is the latent heat of vaporization of the drop and $\boldsymbol{n}_{13}$ is the outward unit vector at the inner interface.

Since we are considering incompressible fluids, the relation between the normal velocities $V_r^{(1)}$ and $V_r^{(2)}$ is obtained from the conservation of mass equation. Neglecting evaporation losses or condensation gains of the liquid phase, we write

$$V_r^{(1)} R_{13}^2 = V_r^{(2)} R_{23}^2, \tag{2}$$

where we make use of the small-capillary-number approximation and consider the normal velocity $V_r^{(1)}$ at the 2–3 interface to be uniform. With the above boundary and interface conditions the problem is fully defined. An analytical solution to the fluid-mechanics part can be found. As far as the heat transfer is concerned, a fully analytical solution does not seem possible even for the case of pure conduction. But

a semi-analytical solution can be found. A fully numerical solution is required when the convective terms are included. Since the problem involves two eccentric non-intersecting spheres the bipolar coordinate system is a natural choice.

2.2. *The bipolar coordinate system*

Introduced by Jeffery (1912), the bipolar coordinate system (ξ, η) is related to cylindrical coordinate system as follows:

$$z = \frac{c \sinh \xi}{\cosh \xi - \cos \eta}, \quad r = \frac{c \sin \eta}{\cosh \xi - \cos \eta}, \tag{3}$$

where c is the half-distance between the points identified by $\xi \to +\infty$ and $\xi \to -\infty$ and constant values of ξ identify non-intersecting eccentric spheres. The 1–3 interface is represented by $\xi = \xi_{13}$ and the 2–3 interface by $\xi = \xi_{23}$. The radii of the interfaces are given by

$$R_{13} = \frac{c}{\sinh \xi_{13}}, \quad R_{23} = \frac{c}{\sinh \xi_{23}}. \tag{4}$$

The distance between the centres of the eccentric spheres is

$$d = R_{23} [\cosh \xi_{23} - R \cosh \xi_{13}], \tag{5}$$

where $R = R_{13}/R_{23}$. We can express ξ_{13} and ξ_{23} in terms of non-dimensional geometric parameters R and (d/R_{23}) as follows:

$$\xi_{13} = \cosh^{-1}\left[\frac{1 - R^2 - (d/R_{23})^2}{2(d/R_{23})\, R}\right], \tag{6}$$

$$\xi_{23} = \cosh^{-1}\left[\frac{1 - R^2 + (d/R_{23})^2}{2(d/R_{23})}\right]. \tag{7}$$

All possible cases may be covered by changing the values of R and (d/R_{23}) or ξ_{13} and ξ_{23}. The eccentricity is defined as a number between 0 and 1 instead of (d/R_{23}) and it is given by

$$\epsilon = \frac{d}{R_{23} - R_{13}}. \tag{8}$$

Now we cast the problem in terms of Stokes stream functions. In the bipolar coordinate system velocities are related to stream functions in the following form:

$$[u_\xi^{(i)}, u_\eta^{(i)}] = \frac{(\cosh \xi - \cos \eta)^2}{c^2 \sin \eta}\left[\frac{\partial \psi^{(i)}}{\partial \eta}, -\frac{\partial \psi^{(i)}}{\partial \xi}\right] \quad (i = 2, 3). \tag{9}$$

With the above representation the continuity equations are identically satisfied. Momentum equations can be satisfied by

$$\mathrm{L}_{-1}^2(\psi^{(i)}) = 0, \tag{10}$$

where L_{-1} is the axisymmetric Stokes operator in the bipolar coordinate system. The boundary/interface conditions may now be expressed in terms of stream functions as

$$\psi^{(2)}|_{\xi,\, \eta \to 0} = \tfrac{1}{2} U c^2 \frac{\sin^2 \eta}{(\cosh \xi - \cos \eta)^2}, \tag{11}$$

$$\left.\frac{\partial \psi^{(2)}}{\partial \eta}\right|_{\xi = \xi_{23}} = \left.\frac{\partial \psi^{(3)}}{\partial \eta}\right|_{\xi = \xi_{23}} = V_r^{(2)} c^2 \frac{\sin \eta}{(\cosh \xi_{23} - \cos \eta)^2}, \tag{12}$$

$$\left.\frac{\partial\psi^{(2)}}{\partial\xi}\right|_{\xi=\xi_{23}} = \left.\frac{\partial\psi^{(3)}}{\partial\xi}\right|_{\xi=\xi_{23}}, \tag{13}$$

$$\mu_2\,\Upsilon(\psi^{(2)})|_{\xi=\xi_{23}} = \mu_3\,\Upsilon(\psi^{(3)})|_{\xi=\xi_{23}}, \tag{14}$$

$$\psi^{(3)}|_{\xi=\xi_{13}} = \tfrac{1}{2}Vc^2\frac{\sin^2\eta}{(\cosh\xi_{13}-\cos\eta)^2}, \tag{15}$$

$$\left.\frac{\partial\psi^{(3)}}{\partial\eta}\right|_{\xi=\xi_{13}} = V_r^{(1)}c^2\frac{\sin\eta}{(\cosh\xi_{13}-\cos\eta)^2}, \tag{16}$$

$$\Upsilon(\psi^{(3)})|_{\xi=\xi_{13}} = 0. \tag{17}$$

where

$$\Upsilon \equiv \frac{1}{c^3}\left\{\frac{\partial}{\partial\eta}\left[\frac{(\cosh\xi-\cos\eta)^3}{\sin\eta}\right]\frac{\partial}{\partial\eta} - \frac{\partial}{\partial\xi}\left[\frac{(\cosh\xi-\cos\eta)^3}{\sin\eta}\right]\frac{\partial}{\partial\xi}\right\},$$

Next, we express the heat-transfer part of the problem in the bipolar coordinate system. Since numerical solution necessitates non-dimensionalization the temperatures are expressed as follows:

$$\Theta_2 = \frac{T_2-T_v}{T_v-T_\infty}, \tag{18}$$

$$\Theta_3 = \frac{T_3-T_v}{T_v-T_\infty}. \tag{19}$$

The energy equations and the boundary/interface conditions are

$$\nabla^2\Theta_i = Pe_i(\cosh\xi-\cos\eta)\left(\frac{R_{23}}{R_{23}^0}\right)\sinh\xi_{23} \times\left[u_\xi^{(i)}\frac{\partial\Theta_i}{\partial\xi}+u_\eta^{(i)}\frac{\partial\Theta_i}{\partial\eta}+\frac{(R_{23}/R_{23}^0)\sinh\xi_{23}}{\cosh\xi-\cos\eta}\frac{\partial T_i^*}{\partial t^*}\right], \tag{20}$$

where

$$\nabla^2 \equiv \frac{(\cosh\xi-\cos\eta)^3}{\sin\eta}\left[\frac{\partial}{\partial\eta}\left(\frac{\sin\eta}{\cosh\xi-\cos\eta}\frac{\partial}{\partial\eta}\right)+\frac{\partial}{\partial\xi}\left(\frac{\sin\eta}{\cosh\xi-\cos\eta}\frac{\partial}{\partial\xi}\right)\right]. \tag{21}$$

The Péclet numbers Pe_i and the dimensionless time t^* are defined as

$$Pe_i = \frac{V_{\text{ref}}R_{23}^0}{k_i/(c_p\rho)_i}, \tag{22}$$

$$t^* = \frac{tR_{23}^0}{V_{\text{ref}}}, \tag{23}$$

where superscript 0 denotes the initial conditions and V_{ref} is a reference velocity that will be defined later. The boundary and interface conditions are

$$\Theta_2|_{\xi,\,\eta\to 0} = -1, \tag{24}$$

$$\Theta_2|_{\xi=\xi_{23}} = \Theta_3|_{\xi=\xi_{23}}, \tag{25}$$

$$k_3\left.\frac{\partial\Theta_3}{\partial\xi}\right|_{\xi=\xi_{23}} = k_2\left.\frac{\partial\Theta_2}{\partial\xi}\right|_{\xi=\xi_{23}}, \tag{26}$$

$$\Theta_3|_{\xi=\xi_{13}} = 0. \tag{27}$$

The relation between the radial velocity $V_r^{(1)}$ and the dimensionless temperature distribution Θ_3 is given by

$$V_r^{(1)} = \frac{\sinh^2 \xi_{13}\, k_3 (T_v - T_\infty)}{2\rho_1 L_3 c} \int_0^\pi \frac{\partial \Theta_3}{\partial \xi} \frac{\sin \eta}{\cosh \xi_{23} - \cos \eta} \mathrm{d}\eta. \tag{28}$$

2.3. *Solution*

2.3.1. *Fluid mechanics*

The general solution to $\mathrm{L}^2_{-1}(\psi^{(i)}) = 0$ is given by Stimson & Jeffery (1926) in the following form:

$$\psi^{(i)}(\xi, \eta) = (\cosh \xi - \cos \eta)^{-\frac{3}{2}} \sum \Xi_n^{(i)}(\xi)\, C_{n+1}^{-\frac{1}{2}}(\cos \eta). \tag{29}$$

Here $C_{n+1}^{-\frac{1}{2}}(\cos \eta)$ is the Gegenbauer polynomial of order $(n+1)$ and degree $-\frac{1}{2}$ and

$$\Xi_n^{(i)}(\xi) = A_n^{*(i)} \cosh (n-\tfrac{1}{2})\xi + B_n^{*(i)} \sinh (n-\tfrac{1}{2})\xi + C_n^{*(i)} \cosh (n+\tfrac{3}{2})\xi + D_n^{*(i)} \sinh (n+\tfrac{3}{2})\xi, \tag{30}$$

where $A_n^{*(i)}, B_n^{*(i)}, C_n^{*(i)}, D_n^{*(i)}$ represent integration constants.

Stimson & Jeffery did not specify the lower limit of the summation in the general series solution. Many other investigators have assumed it to be zero. However, we checked the validity of series and found after some tedious algebra that, in general, it should start from -1, especially if there is growth or collapse. But a close examination reveals that the two leading terms ($n = -1, 0$) each introduce a line source along the z-axis in the solution, in that

$$\left.\frac{\partial \psi^{(i)}}{\partial \xi}\right|_{\eta = 0, \pi} \neq 0. \tag{31}$$

Nevertheless, a suitable relationship between them eliminates the problem and leaves only a point source as required for a growing bubble. The proper general solution can be written as

$$\psi^{(i)}(\xi, \eta) = (\cosh \xi - \cos \eta)^{-\frac{3}{2}} \sum_{n=-1}^{\infty} \Xi_n^{(i)}(\xi)\, C_{n+1}^{-\frac{1}{2}}(\cos \eta), \tag{32}$$

where

$$\Xi_{-1}^{i}(\xi) = A^{*(i)}[\cosh (-\tfrac{3}{2}\xi) + 3 \cosh \tfrac{1}{2}\xi] + B^{*(i)}[-\sinh (-\tfrac{3}{2}\xi) - 3 \sinh \tfrac{1}{2}\xi],$$

$$\Xi_0^{i}(\xi) = A^{*(i)}[\cosh \tfrac{3}{2}\xi + 3 \cosh (-\tfrac{1}{2}\xi)] - B^{*(i)}[\sinh \tfrac{3}{2}\xi + 3 \sinh (-\tfrac{1}{2}\xi)],$$

and $\Xi_n^{(i)}(\xi)$ for $n = 1, 2, \ldots$ is given by (30). Here $A^{*(i)}$ and $B^{*(i)}$ are integration constants.

At this point it should be recognized that the complete solution should be a linear combination of solutions proportional to the velocities U, V and $V_r^{(1)}$ so that the stream functions $\psi^{(i)}$ can be broken into three parts as follows:

$$\psi^{(i)} = Uc^2 \psi_U^{(i)} + Vc^2 \psi_V^{(i)} + V_r^{(1)} c^2 \psi_{V_r}^{(i)}. \tag{33}$$

By letting the viscosity of fluid 1 go to zero in the three-fluid solution given by Sadhal & Oğuz (1985), $\psi_U^{(i)}$ and $\psi_V^{(i)}$ can be obtained. For the present case we take advantage of the simplifications resulting from the zero-shear-stress condition at $\xi = \xi_{13}$. Consequently, the integration constants are not as complex as the three-fluid solution and are given in the Appendices A and B. For the solution involving radial velocities we first redefine the interface conditions (12) and (16) by integrating with respect to

$\cos\eta$. This is done to avoid derivatives of $\psi^{(i)}$ in the boundary conditions. The integration gives

$$\psi^{(2)}_{V_r}|_{\xi=\xi_{23}} = \psi^{(3)}_{V_r}|_{\xi=\xi_{23}} = -\frac{V_r^{(2)}/V_r^{(1)}}{(\cosh\xi_{23}-\cos\eta)} + B', \tag{34}$$

$$\psi^{(3)}_{V_r}|_{\xi=\xi_{13}} = -\frac{1}{(\cosh\xi_{13}-\cos\eta)} + A', \tag{35}$$

where A' and B' are integration constants. Since these constants resulted from the integration of the boundary condition, their values can be obtained by satisfying these conditions at the suitable points ($\eta = 0, \pi$) on each boundary. As a result we get

$$2\sqrt{2}A^{*(2)} = 2\sqrt{2}A^{*(3)} = -\frac{V_r^{(2)}/V_r^{(1)}}{\cosh\xi_{23}+1} + B', \tag{36}$$

$$2\sqrt{2}B^{*(2)} = 2\sqrt{2}B^{*(3)} = -\frac{V_r^{(2)}/V_r^{(1)}}{\cosh\xi_{23}-1} + B', \tag{37}$$

$$2\sqrt{2}A^{*(3)} = -\frac{1}{\cosh\xi_{13}+1} + A', \tag{38}$$

$$2\sqrt{2}B^{*(3)} = -\frac{1}{\cosh\xi_{13}-1} + A'. \tag{39}$$

For six unknowns we have six equations and an additional boundary condition for the proper behaviour of $\psi^{(2)}$ as $\xi\to-\infty$. This condition is met by having $A^{*(2)} = -B^{*(2)}$.

Here we can confirm that $V_r^{(2)}$ and $V_r^{(1)}$ cannot be arbitrary. By solving the above equations with $V_r^{(2)} = R^2 V_r^{(1)}$ the constants are found to be

$$A' = \frac{\cosh\xi_{13}}{\sinh^2\xi_{13}}, \quad B' = \frac{\cosh\xi_{23}}{\sinh^2\xi_{13}}, \tag{40}$$

$$A^{*(2)} = -B^{*(2)} = A^{*(3)} = -B^{*(3)} = \frac{1}{2\sqrt{2}\sinh^2\xi_{13}}. \tag{41}$$

Now we apply the usual procedure of satisfying boundary and interface conditions by expressing them in terms of series and matching them term by term. The boundary and interface conditions become

$$\Xi_n^{(2)}(\xi) < \infty \quad \text{as } \xi\to-\infty, \tag{42}$$

$$\Xi_n^{(2)}(\xi_{23}) = \Xi_n^{(3)}(\xi_{23}) = -\frac{R^2}{\sqrt{2}}\,\mathrm{e}^{-(n+\frac{1}{2})\xi_{23}} - \frac{3B'}{4\sqrt{2}}\left[\frac{\mathrm{e}^{-(n-\frac{1}{2})\xi_{23}}}{n-\frac{1}{2}} - \frac{\mathrm{e}^{-(n+\frac{3}{2})\xi_{23}}}{n+\frac{3}{2}}\right], \tag{43}$$

$$\left.\frac{\mathrm{d}\Xi_n^{(2)}(\xi)}{\mathrm{d}\xi}\right|_{\xi=\xi_{23}} = \left.\frac{\mathrm{d}\Xi_n^{(3)}(\xi)}{\mathrm{d}\xi}\right|_{\xi=\xi_{23}}, \tag{44}$$

$$\mu_2\, Y_\xi\{\Xi_n^{(2)}(\xi), R^2, B'\}_{\xi=\xi_{23}} = \mu_3\, Y_\xi\{\Xi_n^{(3)}(\xi), R^2, B'\}_{\xi=\xi_{23}} \tag{45}$$

$$\Xi_n^{(3)}(\xi_{13}) = -\frac{1}{\sqrt{2}}\,\mathrm{e}^{-(n+\frac{1}{2})\xi_{23}} - \frac{3A'}{4\sqrt{2}}\left[\frac{\mathrm{e}^{-(n-\frac{1}{2})\xi_{23}}}{n-\frac{1}{2}} - \frac{\mathrm{e}^{-(n+\frac{3}{2})\xi_{23}}}{n+\frac{3}{2}}\right], \tag{46}$$

$$Y_\xi\{\Xi_n^{(3)}(\xi), 1, A'\}_{\xi=\xi_{13}} = 0, \tag{47}$$

where

$$Y_\xi\{f(\xi), V, C\} = \frac{\mathrm{d}^2 f(\xi)}{\mathrm{d}\xi^2} + (n-\tfrac{1}{2})(n+\tfrac{3}{2}) f(\xi)$$
$$-(2n+1)\left\{\frac{3V}{2\sqrt{2}\sinh\xi}[(n+\tfrac{3}{2})\,\mathrm{e}^{-(n-\frac{1}{2})\xi} - (n-\tfrac{1}{2})\,\mathrm{e}^{-(n+\frac{3}{2})\xi}]\right.$$
$$\left. -\frac{3C}{4\sqrt{2}}[\mathrm{e}^{-(n-\frac{1}{2})\xi} - \mathrm{e}^{-(n+\frac{3}{2})\xi}]\right\},$$

The above conditions should be satisfied for $n = -1, 0, 1, 2, \ldots$. But we have already calculated the integration constants for the first two terms. A little algebra shows that previously found constants actually satisfy all the above boundary/interface conditions for $n = -1, 0$. Now we need to find the rest of the integration constants. We choose following special forms for $\Xi_n^{(i)}(\xi)$ $(n \geqslant 1)$ which satisfy (42), (43) and (46):

$$\Xi_n^{(2)}(\xi) = A_n[\mathrm{e}^{(n-\frac{1}{2})(\xi-\xi_{23})} - \mathrm{e}^{(n+\frac{3}{2})(\xi-\xi_{23})}] + B_n\,\mathrm{e}^{(n-\frac{1}{2})(\xi-\xi_{23})}, \tag{48}$$

$$\Xi_n^{(3)}(\xi) = C_n\left[\frac{\sinh(n-\frac{1}{2})(\xi-\xi_{23})}{\sinh(n-\frac{1}{2})(\xi_{13}-\xi_{23})} - \frac{\sinh(n+\frac{3}{2})(\xi-\xi_{23})}{\sinh(n+\frac{3}{2})(\xi_{13}-\xi_{23})}\right]$$
$$+ D_n\left[\frac{\sinh(n-\frac{1}{2})(\xi_{13}-\xi)}{\sinh(n-\frac{1}{2})(\xi_{13}-\xi_{23})} - \frac{\sinh(n+\frac{3}{2})(\xi_{13}-\xi)}{\sinh(n+\frac{3}{2})(\xi_{13}-\xi_{23})}\right]$$
$$+ E_n\frac{\sinh(n-\frac{1}{2})(\xi-\xi_{23})}{\sinh(n-\frac{1}{2})(\xi_{13}-\xi_{23})} + B_n\frac{\sinh(n-\frac{1}{2})(\xi_{13}-\xi)}{\sinh(n-\frac{1}{2})(\xi_{13}-\xi_{23})}, \tag{49}$$

where

$$B_n = -\frac{R^2}{\sqrt{2}}\,\mathrm{e}^{-(n+\frac{1}{2})\xi_{23}} - \frac{3B'}{4\sqrt{2}}\left[\frac{\mathrm{e}^{-(n-\frac{1}{2})\xi_{23}}}{n-\frac{1}{2}} - \frac{\mathrm{e}^{-(n+\frac{3}{2})\xi_{23}}}{n+\frac{3}{2}}\right],$$

$$E_n = -\frac{1}{\sqrt{2}}\,\mathrm{e}^{-(n+\frac{1}{2})\xi_{13}} - \frac{3A'}{4\sqrt{2}}\left[\frac{\mathrm{e}^{-(n-\frac{1}{2})\xi_{13}}}{n-\frac{1}{2}} - \frac{\mathrm{e}^{-(n+\frac{3}{2})\xi_{13}}}{n+\frac{3}{2}}\right].$$

We can obtain C_n by satisfying (47) and the use of (44) and (45) gives A_n and D_n.

The solution obtained from the above procedure is added to the solutions proportional to U and V. At this point we have to specify U, V and $V_r^{(1)}$ to have a complete solution. The translational velocities U and V will be obtained from the viscous force balance equations whereas the radial bubble velocity $V_r^{(1)}$ requires the solution of the heat-transfer problem.

2.3.2. *Heat transfer*

Since we include convective terms in the problem it is obvious that a fully analytical solution is not possible. Even in the case of pure conduction we could not find an exact analytical solution because of the difficulty in satisfying the continuity of heat flow condition at the 2–3 interface. We, nevertheless, attack the conduction problem so as to use the solution for comparison with the convection diffusion problem.

In the limiting case of small Péclet number the problem reduces to the solution of Laplace's equation in the bipolar coordinate system. The general solution is given by

$$\Theta_i = (2\cosh\xi - 2\cos\eta)^{\frac{1}{2}} \sum_{n=0}^{\infty} X_n^{(i)}(\xi)\, P_n(\cos\eta), \tag{50}$$

where $P_n(\cos\eta)$ is the Legendre polynomial of order n and

$$X_n^{(i)}(\xi) = a_n^{*(i)}\cosh(n+\tfrac{1}{2})\xi + b_n^{*(i)}\sinh(n+\tfrac{1}{2})\xi. \tag{51}$$

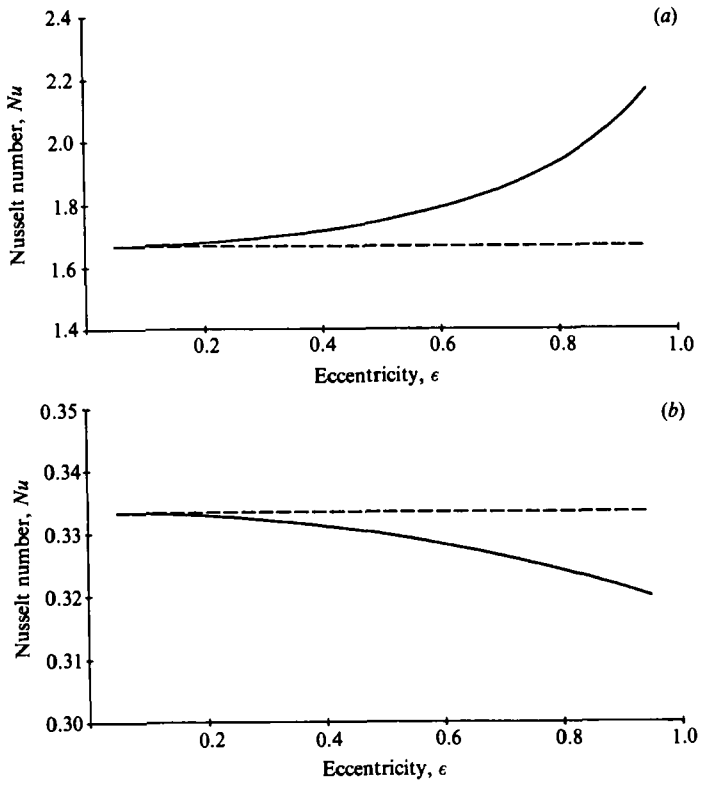

FIGURE 2. Variation of Nusselt number with eccentricity for conductivity ratio: (a) $k_3/k_2 = 0.2$, (b) 5; radius ratio $R = 0.5$: ——, eccentric; --- concentric.

We select following special forms of Θ_i which satisfy (24), (25), (27):

$$\Theta_2 = -1 + (2\cosh\xi - 2\cos\eta)^{\frac{1}{2}} \sum_{n=0}^{\infty} X_n^{(2)}(\xi)\, P_n(\cos\eta) \tag{52}$$

and

$$\Theta_3 = (2\cosh\xi - 2\cos\eta)^{\frac{1}{2}} \sum_{n=0}^{\infty} X_n^{(3)}(\xi)\, P_n(\cos\eta). \tag{53}$$

With the use of the identity

$$\frac{1}{(2\cosh\xi - 2\cos\eta)^{\frac{1}{2}}} = \sum_{n=0}^{\infty} \mathrm{e}^{-(n+\frac{1}{2})\xi} P_n(\cos\eta)$$

we obtain

$$X_n^{(2)}(\xi) = a_n\, \mathrm{e}^{(n+\frac{1}{2})(\xi-\xi_{23})} + \mathrm{e}^{(n+\frac{1}{2})(\xi-2\xi_{23})}$$

and

$$X_n^{(3)}(\xi) = a_n \left[\frac{\sinh(n+\frac{1}{2})(\xi_{13}-\xi)}{\sinh(n+\frac{1}{2})(\xi_{13}-\xi_{23})}\right].$$

The continuity of heat flow condition (26) cannot be satisfied term by term. To find the constants a_n we have to use numerical means. A little algebra leads to the following equation:

$$\sum_{n=0}^{\infty} \left\{\left(\frac{k_3}{k_2} - 1\right)\sinh\xi_{23} - (\cosh\xi_{23} - \cos\eta)(2n+1) \times \left[\frac{k_3/k_2}{\tanh(n+\frac{1}{2})(\xi_{13}-\xi_{23})} + 1\right]\right\} a_n P_n(\cos\eta) = \frac{\sqrt{2}\sinh\xi_{23}}{(\cosh\xi_{23} - \cos\eta)^{\frac{1}{2}}}. \tag{54}$$

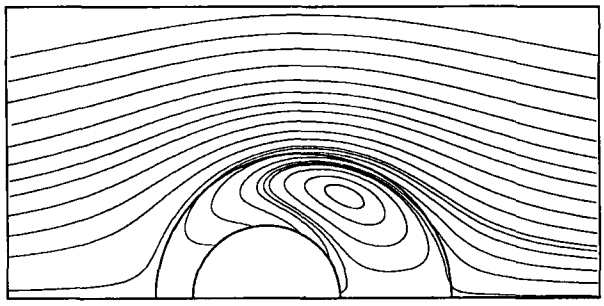

FIGURE 3. Streamlines for a uniform velocity of $U = 1$, a radial velocity of $V_r^{(1)} = 0.1$ and a relative velocity of $V = 0$, with $R = 0.5$, $\epsilon = 0.5$ and $\mu_3/\mu_2 = 0.8$.

The above condition must be met for all a_n. We choose to use the collocation method to calculate the a_n. This method was found to be reasonably easy to apply to this problem. The equation is written at the roots of the Legendre polynomial $P_n(\cos\eta)$ giving N linear equations in the a_n. The number N denotes the highest order of P_N used in the series to approximate the temperature field. The value of N depends on the eccentricity and the conductivity ratio (k_3/k_2) for the desired accuracy. For our calculations, we require $10 \leqslant N \leqslant 40$.

Using (28) in terms of coefficients a_n we can calculate the total heat flow which yields the normal velocity $V_r^{(1)}$,

$$V_r^{(1)} = \sinh^2\xi_{13}\frac{k_3(T_v - T_\infty)}{\rho_1 L_3 c}\sum_{n=0}^{\infty} e^{-(n+\frac{1}{2})\xi_{23}}\frac{a_n}{\sinh(n+\frac{1}{2})(\xi_{13}-\xi_{23})}. \tag{55}$$

The total heat flow is

$$Q = 4\pi c k_3(T_v - T_\infty)\sum_{n=0}^{\infty} e^{-(n+\frac{1}{2})\xi_{23}}\frac{a_n}{\sinh(n+\frac{1}{2})(\xi_{13}-\xi_{23})}, \tag{56}$$

which may be non-dimensionalized by defining the Nusselt number Nu as follows:

$$Nu = \frac{QR_{13}}{k_3(T_v - T_\infty)A}. \tag{57}$$

For the pure-conduction case, Nu is plotted as a function of eccentricity in figure 2(*a*, *b*). For case (*a*), with $k_3/k_2 = 0.2 < 1$, we see an increase in Nu with increasing eccentricity. This is because the thinner region of the film plays the dominant role in determining the resistance. For case (*b*) we have $k_3/k_2 = 5 > 1$. Here the Nusselt number decreases gently with increasing eccentricity. The effect of eccentricity is rather weak because of the high conductivity in phase 3.

The finite-difference formulation of the problem is not as straightforward, as one might think, because of the complexity and non uniformity of the grid in a bipolar coordinate system. The formulation must be suitable for all possible cases. For this reason we used the spherical coordinate system for region 2 and the bipolar coordinate system for region 3. Since the matching is done at the 2–3 interface the origin for the spherical system is taken at the centre of the outer sphere. To obtain uniform grid spacing in the η-direction, we first take a ξ_{avg} which corresponds to an average radius R_{avg}:

$$R_{avg} = \frac{c}{\sinh\xi_{avg}} = \tfrac{1}{2}(R_{23} + R_{13}).$$

Equally spaced points on the arc identified by $\xi = \xi_{avg}$ are taken to obtain discrete η-values which are then matched with discrete θ-values at the 2–3 interface. We used equally spaced points in the ξ- and the radial directions.

Another major difficulty is to take into account the continuously changing geometry. It is very difficult to estimate the time derivative because the configuration of the grid is not the same as it is at the previous time step. For this reason we formulate the problem in a special way. Instead of using grids fixed in space we used infinitesimal volumes moving due to the changing configuration. For each volume cell we write the integral form of the heat equation which involves the time derivative of the heat capacity of the cell and the net heat flow across the cell surfaces. At a given time the total heat flow across a surface is given by the sum of the conductive and convective terms. The convective velocities at the surface are obtained by simply adding the velocity of the flow field to the velocity of the cell surface induced by the moving grid.

In the case of growth, the initial condition is a simple step decrease in temperature at the surface of the bubble and a uniform temperature distribution for the liquid drop and the bulk phase. The surface temperature here corresponds to the equilibrium temperature at the liquid pressure. In the case of collapse, however, we impose a linear temperature distribution in the thin liquid film and a uniform temperature for the bulk phase. This represents an approximation to the actual temperature distribution at the time when the condensate has formed a thin film. The time span for this initial condensation process is sufficiently small that any error caused by the approximation does not seriously affect the time history. Also, from the growth histories we see that for a low-conductivity film, in the final stages of bubble growth it has a radially linear profile. This is partly because, for a thin film, convective circulation is almost absent. This point has been noted earlier by Rushton & Davies (1973) and Sadhal & Oğuz (1985).

There is no particular difficulty in satisfying the boundary and interface conditions. The continuity conditions at the 2–3 interface become a simple energy balance equation (similar to the one used in the bulk phase) with a discontinuity in conductivity.

3. Flow field

For this problem plotting the streamlines is more than just an observation of flow patterns: we can actually get crucial information about the behaviour of the system. We did not put arrows on the streamlines because the flow can be visualized in two ways. For instance one way of looking at figure 3 is to imagine the collapse of the bubble. In this case the uniform stream should be from right to left. On the other hand we can also consider a growth; then the uniform stream should be from left to right. By similar reasoning we can also consider the cases where the eccentric position of the inner sphere is on the right-hand side in the drop. For instance, if we had to reverse figure 3 with respect to the centre we would get streamlines covering the case of a collapse with a uniform stream from left to right. The above reasoning is valid owing to the generality of the solution. In other words, for cases in which the inner sphere is off-centre towards the positive z-direction (i.e. both can be spheres identified by negative values of ξ) we do not have to solve a new problem. The calculation of drag forces in 34 also supports this argument.

In figure 4 streamlines showing various cases of collapse have been plotted. The effect of the relative velocity V is very clear from the plots. For the case $V = 0.2$ and

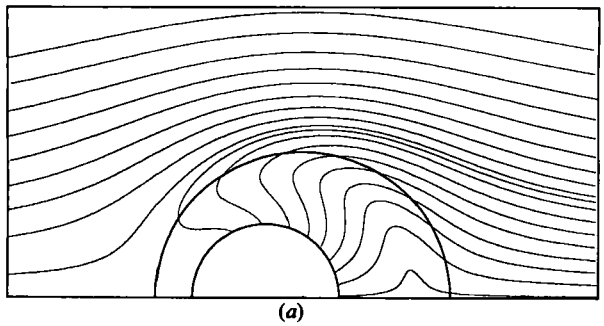

(*a*)

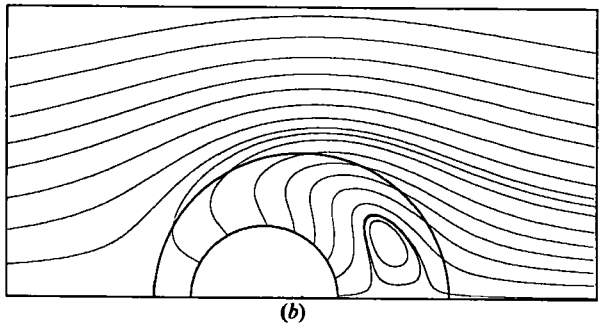

(*b*)

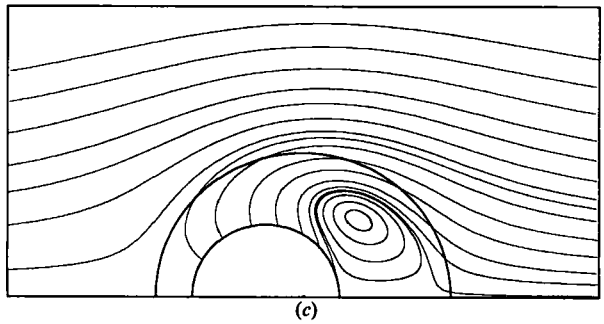

(*c*)

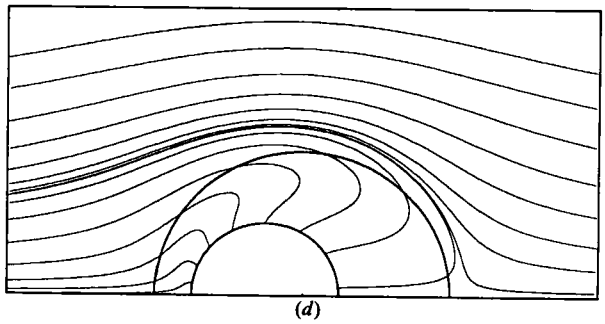

(*d*)

FIGURE 4. The effect of the relative velocity V for the case $U = 1$, $V_r^{(1)} = 0.2$ with $R = 0.5$, $\epsilon = 0.5$ and $\mu_3/\mu_2 = 0.8$. (*a*) $V = 0.2$, (*b*) 0, (*c*) -0.2; and (*d*) $V = -0.2$ and $V_r^{(1)} = -0.2$.

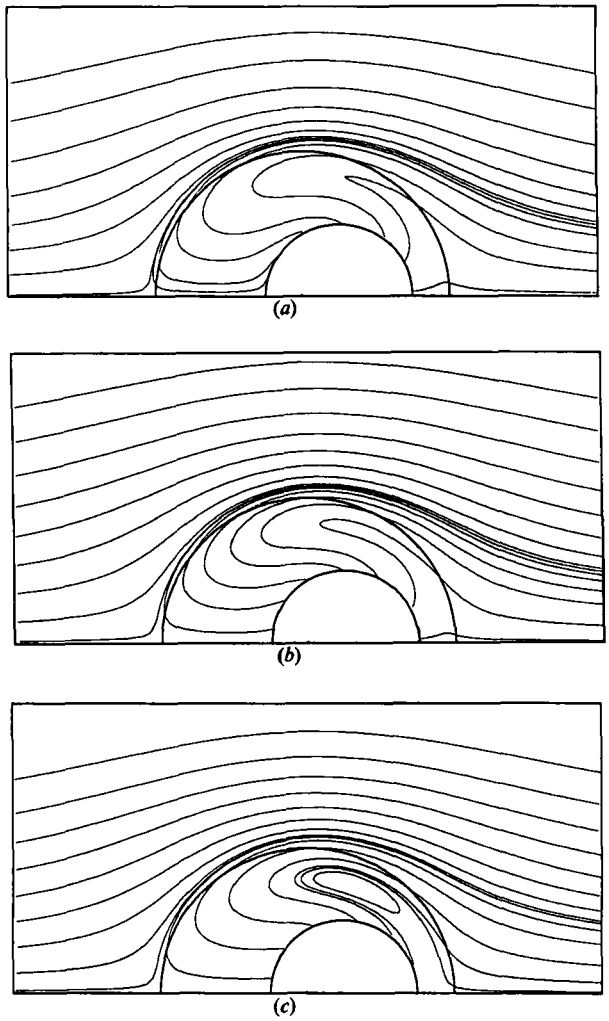

FIGURE 5. Streamlines for the case of a bubble with its centre to the right of the outer sphere centre: $U = 1$, $V_r^{(1)} = -0.1$ with $R = 0.5$, $\epsilon = 0.5$ and $\mu_3/\mu_2 = 0.5$. (*a*) $V = 0.1$, (*b*) 0, (*c*) -0.1.

$V_r^{(1)} = 0.2$ the velocity on the left stagnation point of the bubble is zero and no strong internal circulation is observed. Whereas in the case when $V = 0$ a cell appears on the right of the bubble. It becomes larger when $V = -0.2$ making the normal velocity on the right stagnation point zero. For all of the above cases the location of the vortex did not change significantly. For the same configuration in the case $V_r^{(1)} = -0.2$ and $V = 0.2$ we get figure 4(*d*). Although no internal circulation is observed, it is clear from the flow patterns that growth shifts the vortex from right to left in the case of a uniform stream in the opposite direction.

Figure 5 shows the cases in which the internal circulation is in the thinner region of the shell. Again from the streamlines for various values of V it is not difficult to conclude that it is the direction of the radial motion of the interface that controls the position of the cell. Finally figure 6 shows that as the eccentricity decreases, it gives more room for internal circulation on the thinner side of the shell. In the next section we derive the expressions for drag on each sphere and the force balance equations involving the unknown velocities U and V.

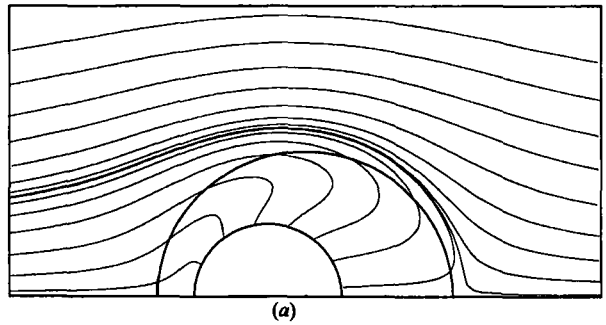

(*a*)

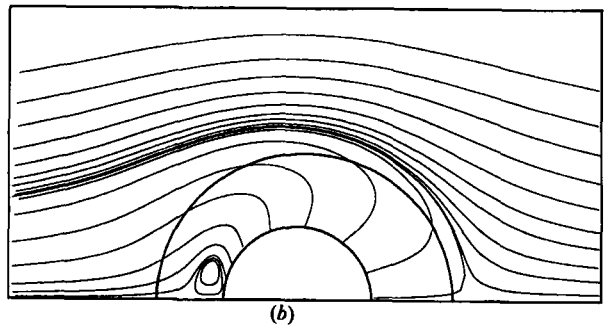

(*b*)

FIGURE 6. The effect of changing eccentricity for the case $U = 1$, $V = -0.2$, $V_r^{(1)} = -0.2$, $R = 0.5$ and $\mu_3/\mu_2 = 2.0$. (*a*) $\epsilon = 0.5$, (*b*) 0.1.

4. Drag and translational velocities

The above solution is not complete unless we calculate the drag on each sphere. Stimson & Jeffery (1926) derived the formula for viscous drag in a bipolar coordinate system. But this formula is not valid if the series begins with $n = -1$. After some lengthy algebra and by using the Symbolic Manipulator Program (SMP) we finally arrived at the following general formula for viscous drag on each sphere identified by positive values of ξ:

$$F_D^{(i)} = -\frac{2\sqrt{2\pi}\mu_i}{c}\left[4A^{*(i)} - 4B^{*(i)} + \sum_{n=1}^{\infty}(A_n^{*(i)} + B_n^{*(i)} + C_n^{*(i)} + D_n^{*(i)})\right], \tag{58}$$

where $F_D^{(2)}$ is the viscous force on the outer sphere and $F_D^{(3)}$ that on the inner one.

Since we neglect inertial terms, only viscous and buoyant forces will be considered in the instantaneous force balance equations in the z-direction. The total viscous force on each sphere has three parts. The first one is induced by the velocity U of the drop and it is proportional to U. The relative velocity V of the bubble with respect to the drop causes the second part of the viscous force and it is proportional to V. As long as there is a non-zero eccentricity, expansion of the bubble contributes to the viscous force in the z-direction. So the third part of viscous force is proportional to $V_r^{(1)}$. With the above considerations instantaneous force balance equations can be written as follows:

outer sphere:

$$\tfrac{4}{3}[\rho_2 R_{23}^3 - \rho_3(R_{23}^3 - R_{13}^3)]g = \alpha_2\mu_2 UR_{23} + \beta_2\mu_2 VR_{23} + \gamma_2\mu_2 V_r^{(1)} R_{23}; \tag{59}$$

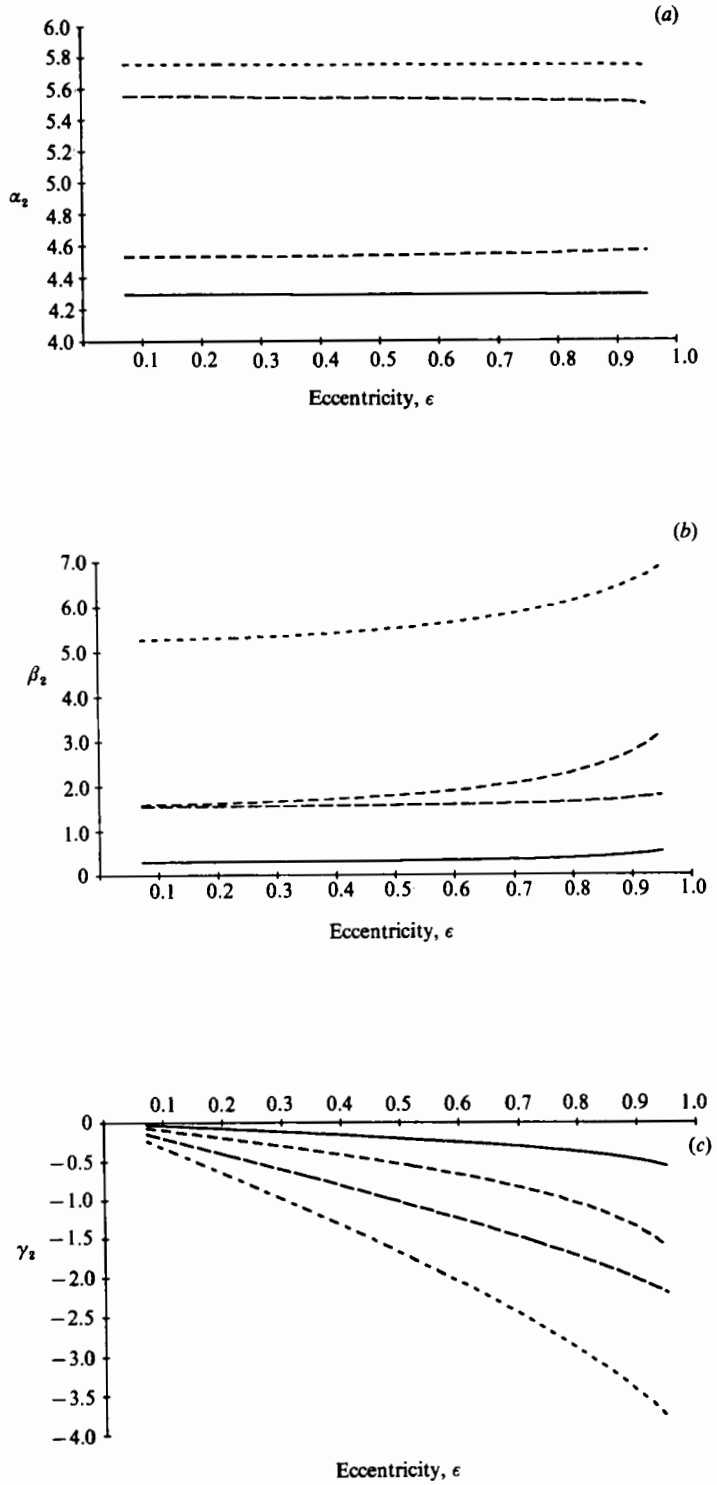

FIGURE 7. The dimensionless drag components acting on the outer sphere as a function of eccentricity. α_2 induced by U, β_2 by V, γ_2 by $V_r^{(1)}$: ——, $R = 0.50$, $\mu_3/\mu_2 = 0.1$; — —, $R = 0.50$, $\mu_3/\mu_2 = 2.0$; – – –, $R = 0.75$, $\mu_3/\mu_2 = 0.1$; - - -, $R = 0.75$, $\mu_3/\mu_2 = 2.0$.

inner sphere:

$$\tfrac{4}{3}\rho_3 R_{13}^3 g = \alpha_3 \mu_2 U R_{23} + \beta_3 \mu_2 V R_{23} + \gamma_3 \mu_2 V_r^{(1)} R_{23}; \tag{60}$$

where α_i, β_i and γ_i represent non-dimensional viscous drag components corresponding to U, V and $V_r^{(1)}$, respectively. The expressions for these components are given in the Appendices. The densities of the respective phases are given by ρ_i and the gravitational acceleration by g.

Before we solve the above system for U and V it is convenient to put the equations in non-dimensional form. Since the radius of the drop changes we use the initial radius of the drop denoted by R_{23}^0 as a lengthscale. Then the force balance equations become:

outer sphere:

$$\tfrac{4}{3}[1-\rho(1-R^3)] = [\alpha_2 U^* + \beta_2 V^* + \gamma_2 V_r^{(1)*}](R_{23}^0/R_{23})^2, \tag{61}$$

inner sphere:

$$\tfrac{4}{3}\rho R^3 = [\alpha_3 U^* + \beta_3 V^* + \gamma_3 V_r^{(1)*}](R_{23}^0/R_{23})^2, \tag{62}$$

where $\rho = \rho_3/\rho_2$ and a reference velocity V_{ref} is defined such that

$$U^* = U/V_{\text{ref}}, \tag{63}$$

$$V^* = V/V_{\text{ref}}, \tag{64}$$

$$V_r^{(1)*} = V_r^{(1)}/V_{\text{ref}}, \tag{65}$$

$$V_{\text{ref}} = \rho_2 g R_{23}^{(0)2}/\mu_2. \tag{66}$$

The solution of the above system of linear equations gives the instantaneous velocities U and V.

The dimensionless drag coefficients α_i, β_i and γ_i are plotted in figures 7 and 8 for the outer and inner spheres respectively. In these plots a positive drag coefficient represents a force in the negative z-direction. Here the sign convention for the unit velocities is as follows: translational velocities are in the direction of negative z-axis and radial velocities are in the direction towards the centre. It can be noted that increasing viscosity and/or radius ratio always increases the magnitude of these coefficients. The effect of increasing the ratio is that the liquid film in phase 3 becomes thinner, thereby increasing the resistance to its internal circulation. This leads to an increased drag. In the range covered by the graphs the coefficients did not change sign. A careful observation shows that the coefficients γ_i (induced by radial velocity) are odd functions of the eccentricity whereas the coefficients α_i and β_i (induced by translational velocities) are even functions. Here we note that an outward radial velocity of the inner interface creates a force towards the centre of the outer sphere. This is probably the result of an increased pressure in the thinner region of the film which may cause the inner sphere to move towards the centre of the outer sphere. By the same token an inward radial velocity forces the inner sphere away from the centre. However, this does not mean that outward radial velocity stabilizes the configuration. From a purely geometrical argument, eccentricity increases with bubble growth in the absence of relative translational motion between the bubble and the drop.

At a given time and configuration the instantaneous velocity calculation involves an iterative process for radial velocity. The radial velocity given by the solution is then substituted into the force balance equations to calculate the translational velocities U^* and V^*. Having found $V_r^{(1)*}$, U^* and V^* the flow field is fully defined. We further solve the convection–conduction equation by using a finite-difference formulation. From the solution the total heat flow into the bubble can be calculated.

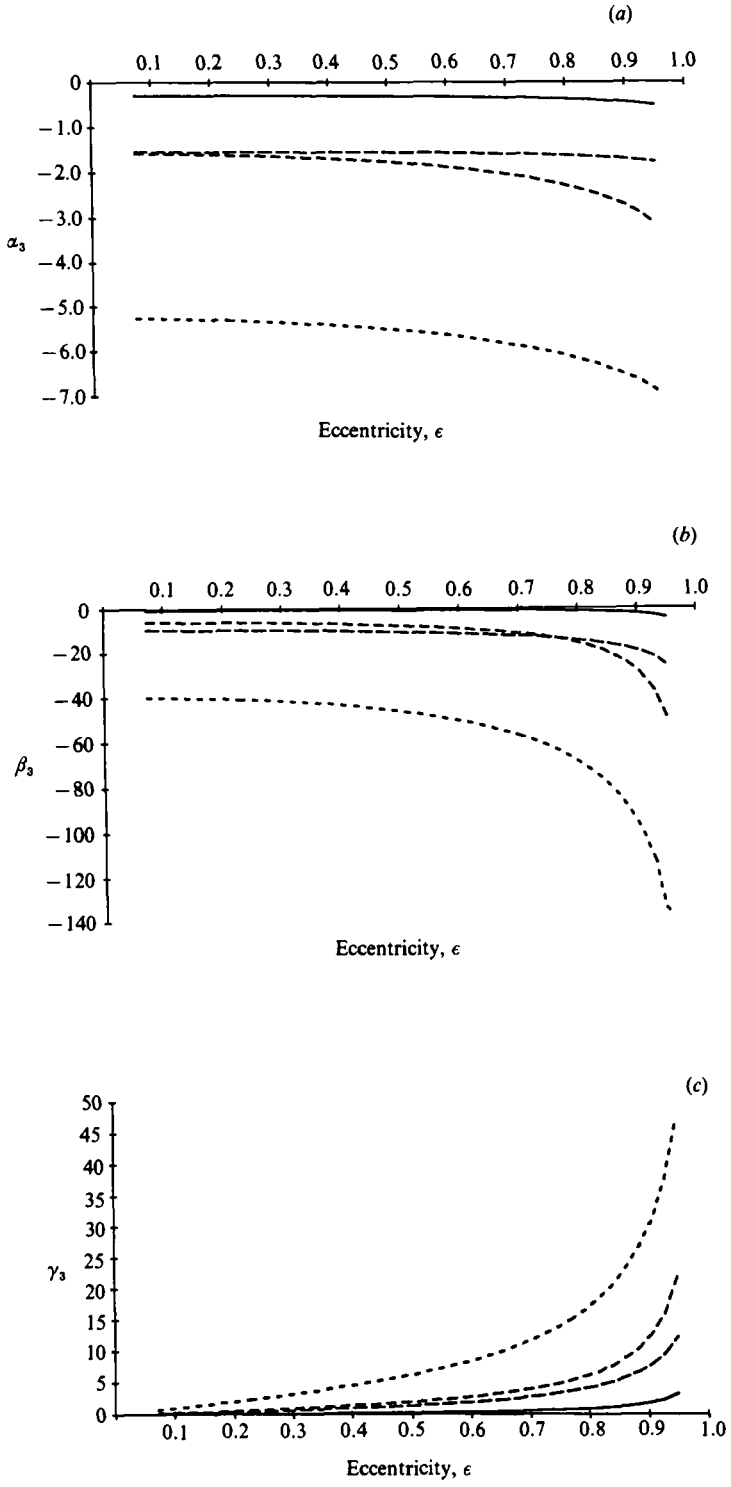

FIGURE 8. The dimensionless drag components acting on the inner sphere as a function of eccentricity. α_3 induced by U, β_3 by V, γ_3 by $V_r^{(1)}$: ——, $R = 0.50$, $\mu_3/\mu_2 = 0.1$; ——, $R = 0.50$, $\mu_3/\mu_2 = 2.0$; – – –, $R = 0.75$, $\mu_3/\mu_2 = 0.1$; - - -, $R = 0.75$, $\mu_3/\mu_2 = 2.0$.

In terms of the Jakob number,

$$Ja = \frac{c_p(T_v - T_\infty)}{L_3} \tag{67}$$

and Nusselt number Nu the normal velocity $V_r^{(1)*}$ can be written as

$$V_r^{(1)*} = Ja\, Nu \left(\frac{\rho_3}{\rho_1}\right)\left(\frac{R_{23}^0}{R_{13}}\right)\Big/ Pe_3. \tag{68}$$

The radial velocity found from the finite-difference solution is then substituted into the force balance equations to close the iteration cycle. Convergence is reached when changes in velocities are small enough. Since at any given time there is a non-zero radial velocity and hence a continuously changing geometry we cannot talk about the stability of any instantaneous equilibrium configuration. What we can do however is to carry out a time-history analysis. Given an initial configuration and initial parameters the time history of the compound drop can be studied. This is done in the next section.

5. Time histories

The solution obtained above can be used to investigate the motion of the bubble inside the drop. At a given time the velocities are known and the flow is fully developed according to the quasi-steady assumption. To calculate the configuration after an infinitesimal increment of time we simply have to integrate the velocities with respect to time. By repeating this procedure we can get the time history of the compound drop. We stop the process either when the bubble gets very close to the outer interface or in the case of collapse when the radius ratio is sufficiently small.

As mentioned before we are using the initial radius of the drop as a length-scale because it undergoes the least change. The procedure to calculate the configuration involves three dimensionless lengths R_{13}^*, R_{23}^*, D^* to fully define the problem. Here $R_{13}^* = R_{13}/R_{23}^0$, $R_{23}^* = R_{23}/R_{23}^0$, $D^* = d/R_{23}^0$ and d is the distance of the bubble centre from the drop centre. If $R_{13}^{(n)*}$, $R_{23}^{(n)*}$ and $D^{(n)*}$ represent dimensionless lengths at time n then $R_{13}^{(n+1)*}$, $R_{13}^{(n+1)*}$ and $D^{(n+1)*}$ are given by

$$R_{13}^{(n+1)*} = R_{13}^{(n)*} + V_r^{(1)*}\,\Delta t^*, \tag{69}$$

$$R_{23}^{(n+1)*} = R_{23}^{(n)*} + V_r^{(2)*}\,\Delta t^*, \tag{70}$$

$$D^{(n+1)*} = D^{(n)*} + V^*\,\Delta t^*, \tag{71}$$

where Δt^* is a dimensionless increment of time and the dimensionless time t^* is defined as

$$t^* = \frac{tg\rho_2 R_{23}^0}{\mu_2}. \tag{72}$$

Here Euler's formula of numerical integration was used for simplicity. Several runs showed no drastic change in velocities except at the final stage of the collapse of the bubble. We have obtained growth and collapse histories for various cases. The results are discussed below.

5.1. *Growth histories*

The present analysis deals with cases in which the thermodynamic forces favour the nucleation of a vapour bubble within the drop as opposed to the liquid–liquid interface. The low-Reynolds-number assumption limits the results to situations with

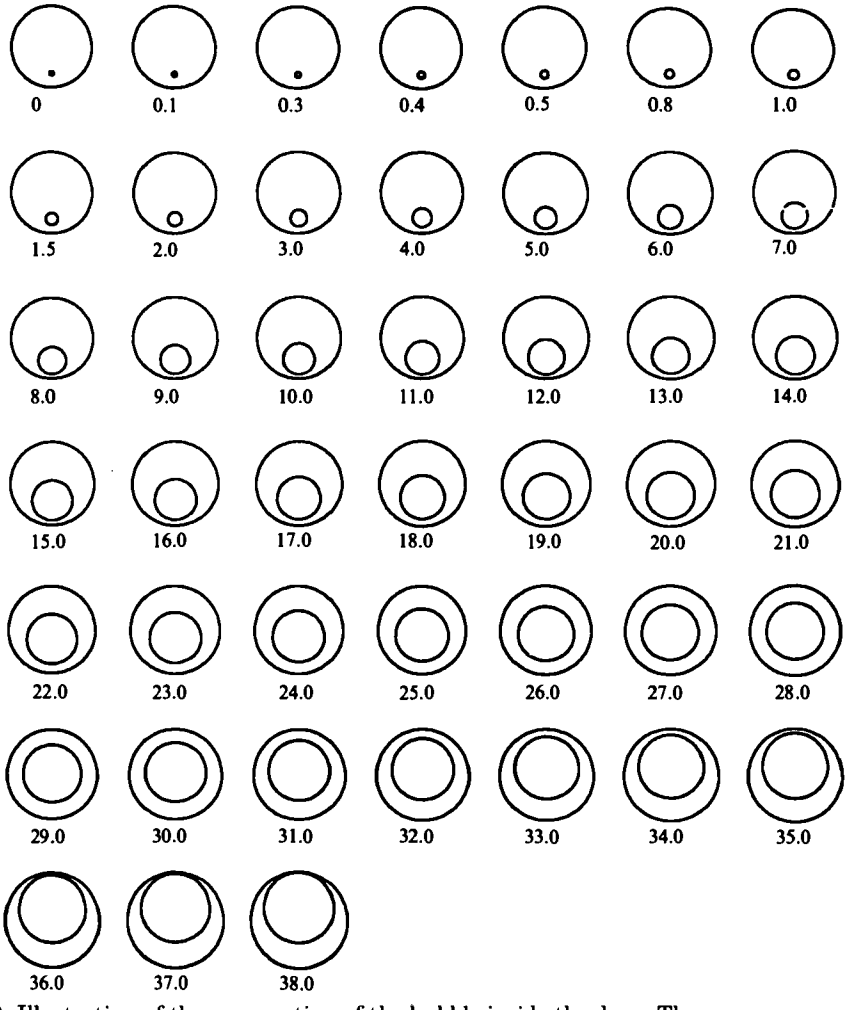

FIGURE 9. Illustration of the evaporation of the bubble inside the drop. The sequences correspond to the configuration of the compound drop at the time t^* given under each one. In this case, $\mu_3/\mu_2 = 2.0$, $\rho_3/\rho_2 = 0.8$, $k_3/k_2 = 0.2$, $\alpha_3/\alpha_2 = 0.2$, $Pe_2 = 0$ and $Ja(\rho_1/\rho_3)/Pe_3 = 0.005$.

small ΔT. In such cases nucleation may be initiated for experimental purposes with very dilute particulate additives.

Previous models and experimental observations of an evaporating two-phase drop suggest the configuration of a bubble partially covered by its liquid phase. This has been observed for both the high- and the low-Reynolds-number cases. The current analysis has in fact showed this to be the tendency of such compound drops even when the bubble nucleates within the drop. From the results we conclude that most of the time the bubble reaches the outer interface favouring a partially covered bubble configuration. Note that the growth of the bubble actually creates a force towards the centre of the drop. But the purely geometrical effect of radial motion of the interface is to increase the eccentricity. Between these two competing mechanisms the radial motion is usually dominant. In addition to the radial growth of the bubble, the translation of the drop creates a force in the upward direction regardless of eccentricity. For this reason the initial position of the bubble inside the drop is very

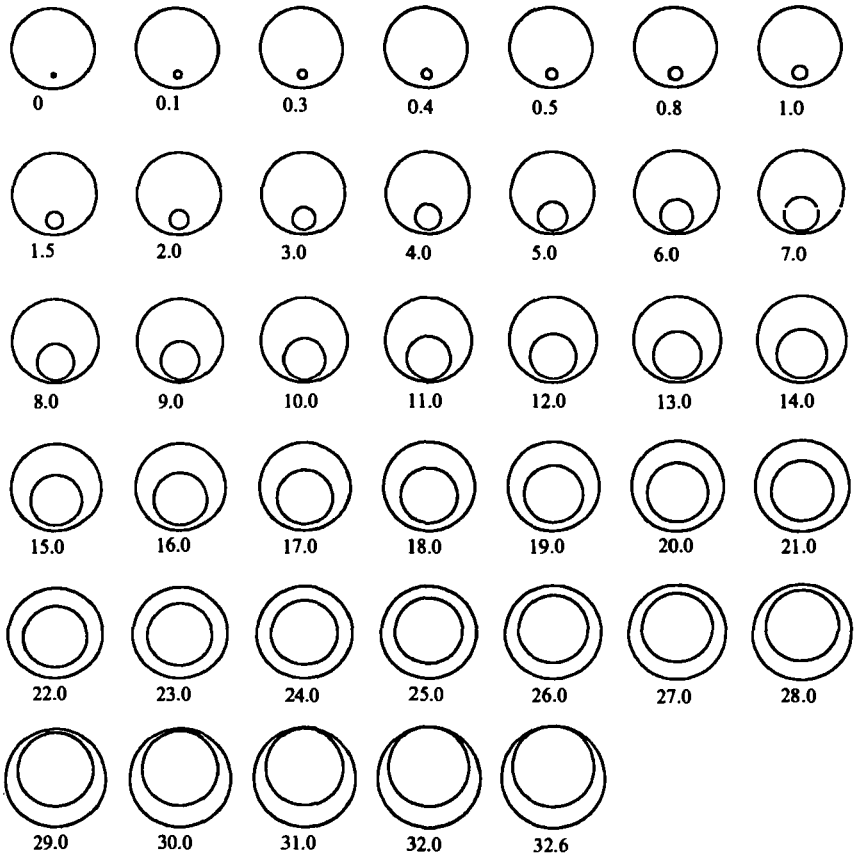

FIGURE 10. The time history for the case $\mu_3/\mu_2 = 2.0$, $\rho_3/\rho_2 = 0.8$, $k_3/k_2 = 0.2$, $\alpha_3/\alpha_2 = 0.2$, $Pe_2 = 8.0$ and $Ja(\rho_1/\rho_3)/Pe_3 = 0.005$.

important for the subsequent behaviour of the configuration. If we begin with a configuration of a bubble close to the top, then after a few time steps the bubble reaches the outer interface. On the other hand, if we place the bubble at the bottom we get the time histories described in figures 9 and 10 which show steady migration from bottom to top. Similar sequences are obtained when we cut the evaporation rate by half. But for this case the bubble stays longer inside the drop. It should be noted that in general the initial bubble position is governed by the thermodynamics and the fluid dynamics prior to nucleation. This prior history has not been taken into consideration in the present analysis. Instead, the histories following a given initial configuration have been obtained.

The dimensionless velocities of the above cases are plotted as functions of time in figure 11. A sharp decrease in radial velocity is observed at the beginning of the evaporation. The continuous increase of the translational velocity U is due to the changing buoyant forces.

The relative velocity V drops considerably before the bubble touches the outer interface 2–3. This is because the drag coefficients get larger in magnitude as the eccentricity increases.

Nusselt number is plotted as a function of time in figure 12 (a, b) for growing

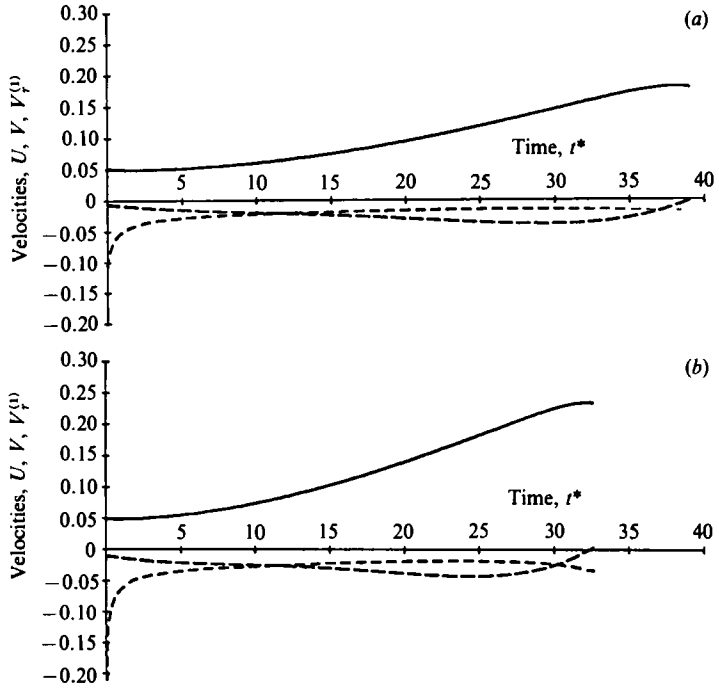

FIGURE 11. Dimensionless velocities for the cases in figures 9 and 10: ——, U; ——, V; ---, $V_r^{(1)}$. (a) $Pe_2 = 0$; (b) $Pe_2 = 8.0$.

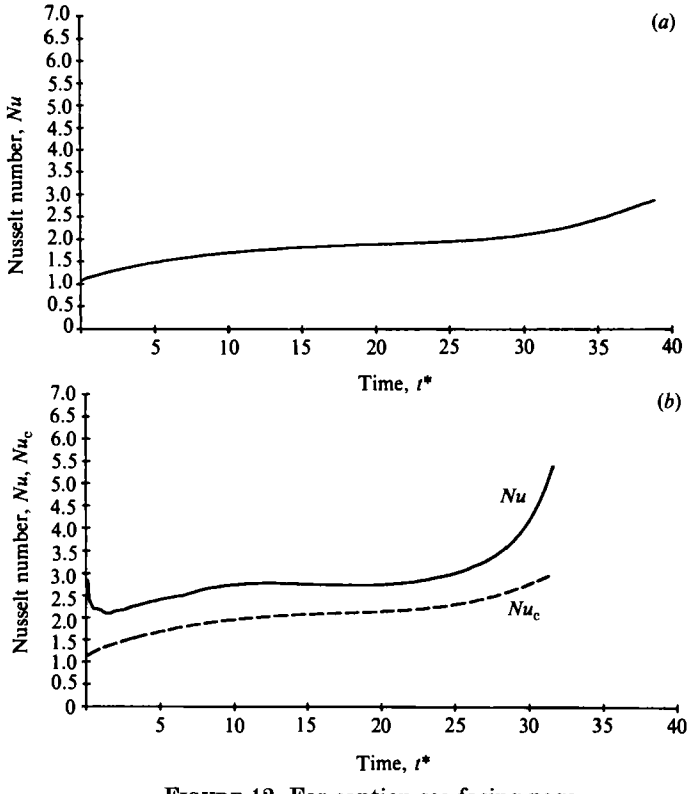

FIGURE 12. For caption see facing page.

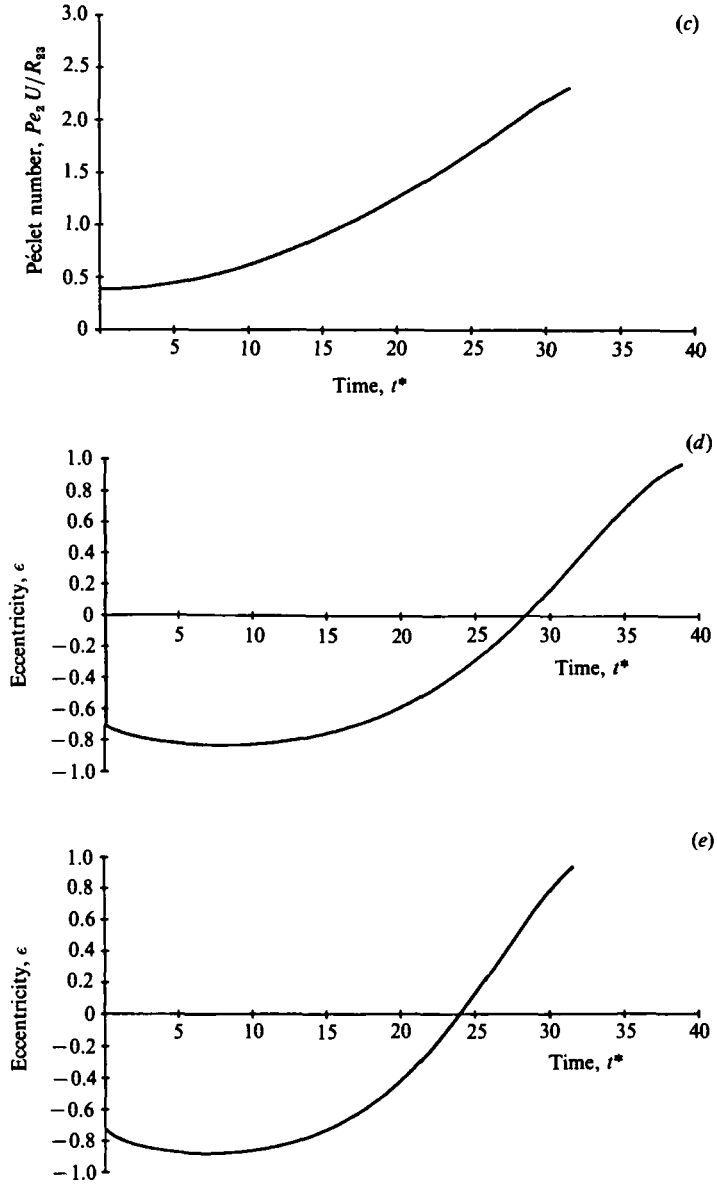

FIGURE 12. (*a*) Nusselt number as a function of time for initial $Pe_2 = 0$; (*b*) Nusselt number as a function of time for initial $Pe_2 = 8$, here Nu_c is the conduction part of the solution. (*c*) Péclet number as a function of time for case (*b*). (*d*) Eccentricity as a function of time for case (*a*) ($Pe_2 = 0$). (*e*) Eccentricity as a function of time for case (*b*) ($Pe_2 = 8$).

bubbles. For the first case (*a*) the Péclet number is taken to be zero. For this case a monotonic increase is observed for the Nusselt number. This is due to the decreasing thickness of the liquid film resulting from growth. This observation is particularly true if the film has a much lower conductivity than the continuous phase. For the second case (figure 12*b*), we include convective terms with an initial Péclet number of 8. On the same graph the pure-conduction part of the Nusselt number Nu_c has

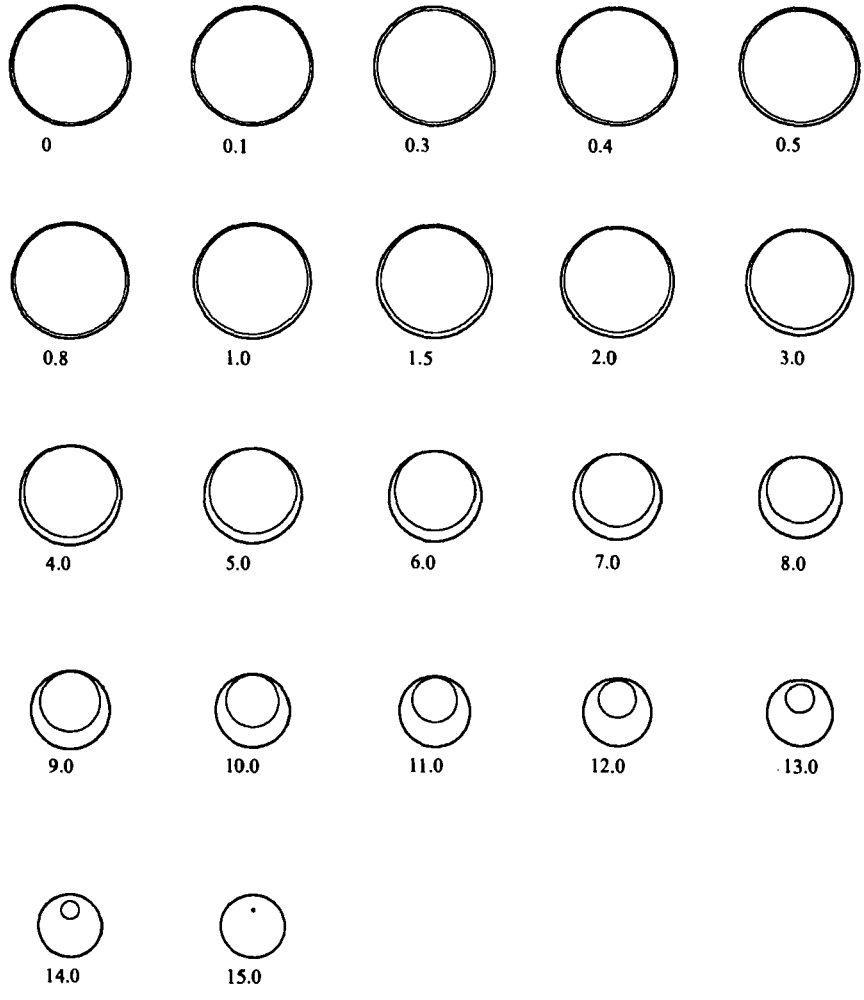

FIGURE 13. The time history for the case $\mu_3/\mu_2 = 2.0$, $\rho_3/\rho_2 = 0.8$, $k_3/k_2 = 0.2$, $\alpha_3/\alpha_2 = 0.2$, $Pe_2 = 0$ and $Ja(\rho_1/\rho_3)/Pe_3 = -0.01$.

been plotted. Here the two solutions at each time step correspond to identical geometrical configurations. Figure 12(*a*), however, relates to a different sequence of configurations because in that case the time history is taken to be governed by pure conduction. In figure 12(*c*) the Péclet number is plotted as a function of time for the case in 12(*b*). Here we see a monotonic increase in Péclet number with time, largely due to the increased buoyancy. In figures 12(*d*, *e*) the eccentricities are plotted as a function of time for the cases corresponding to figures 12(*a*, *b*), respectively. The eccentricity is a measure of the distance between the centres of the inner and the outer spheres as defined in (8). It is inferred from this plot that a steady motion of the bubble relative to the drop takes place for moderate eccentricities. We discuss the cases of bubble collapse next.

5.2. *Collapse histories*

Figures 13 and 14 show the sequences of bubble collapse starting with zero eccentricity. In this case, when the heat transfer rate is high enough the bubble always

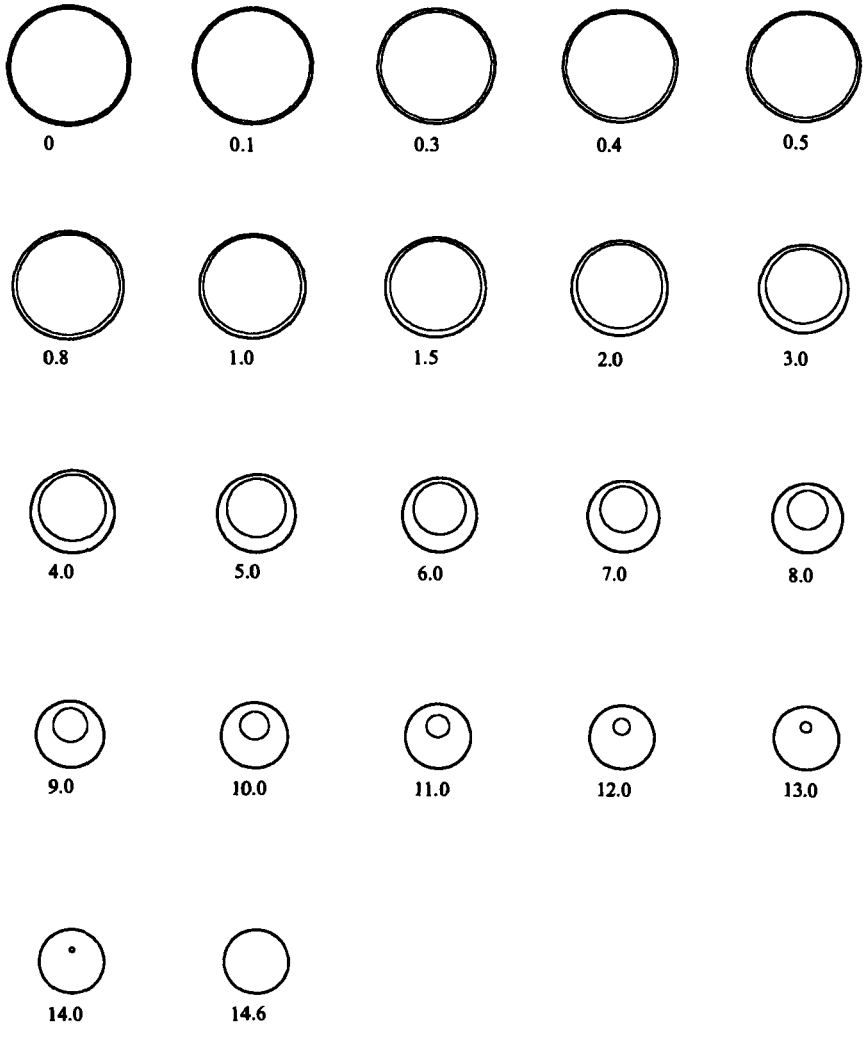

FIGURE 14. The time history for the case $\mu_3/\mu_2 = 2.0$, $\rho_3/\rho_2 = 0.8$, $k_3/k_2 = 0.2$, $\alpha_3/\alpha_2 = 0.2$, $Pe_2 = 40$ and $Ja(\rho_1/\rho_3)/Pe_3 = -0.01$.

stays inside the drop until it finally disappears. Note that the radial velocity creates a force out of the centre of the drop. But the relative translational velocity is not high enough to lead to a partially covered bubble because of rapid shrinkage.

We examine the velocities in figure 15. The radial velocity is, of course, just the reverse of the previous case. The velocity of the drop and the relative velocity of the bubble decrease as the bubble gets smaller. This is simply due to the changes in buoyant forces. In figure 16 (*a*, *b*) the Nusselt number is plotted as a function of time. As in figure 12, the first case (*a*) represents $Pe_2 = 0$ and in the second one (figure 16*b*) the initial Péclet number is 40. For the second case we also give the conduction part of the Nusselt number for comparison purposes. As in the case of evaporation, the radial convective terms work against conduction and decrease Nu. In figure 16 (*c*) the Péclet number is given as a function of time for the case in figure 16 (*b*). It decreases monotonically with time as the buoyancy-driven translational velocity decreases with collapse. The variation of eccentricity with time for the cases in figures 16 (*a*, *b*)

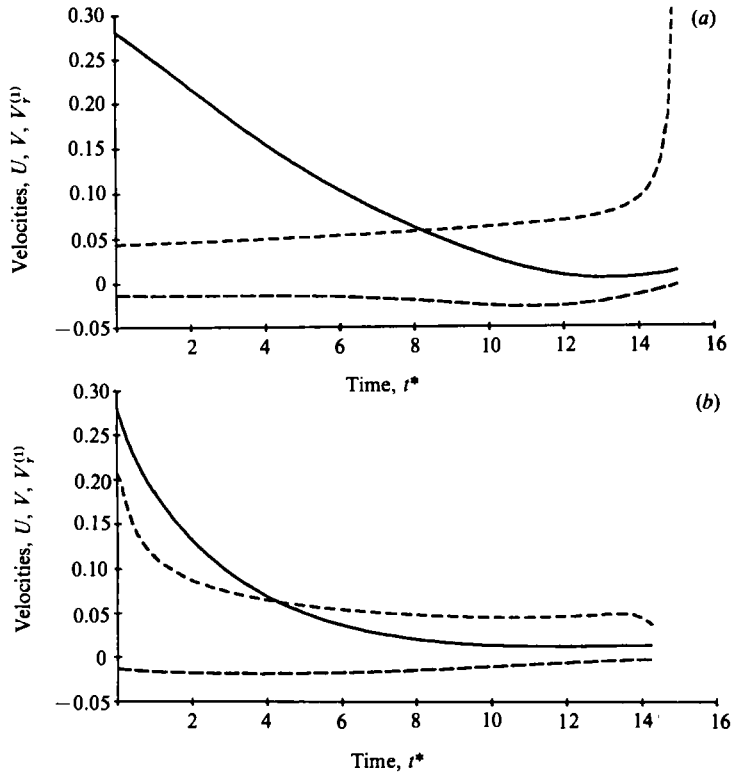

FIGURE 15. Dimensionless velocities for the cases in figures 13 and 14: ——, U; — —, V; – – –, $V_r^{(1)}$. (*a*) $Pe_2 = 0$; (*b*) $Pe_2 = 40$.

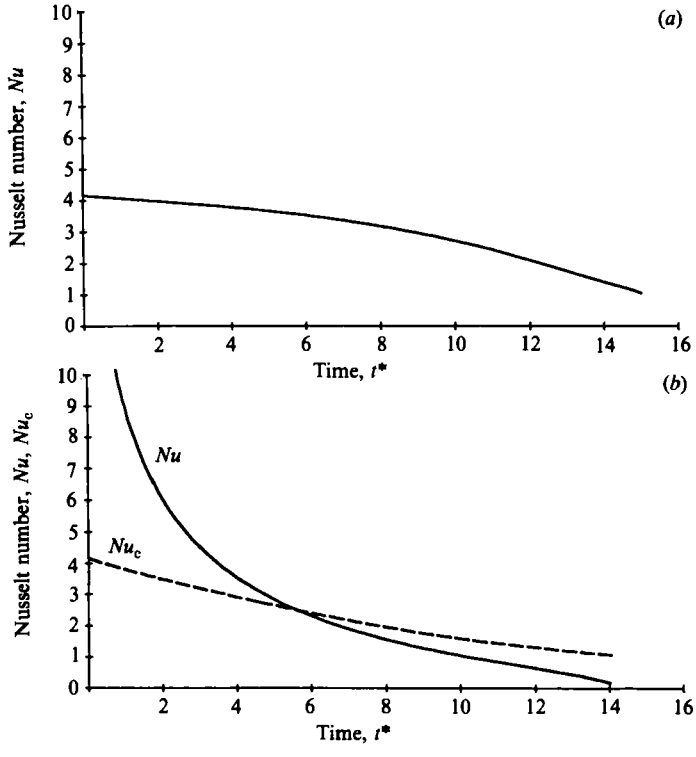

FIGURE 16. For caption see facing page.

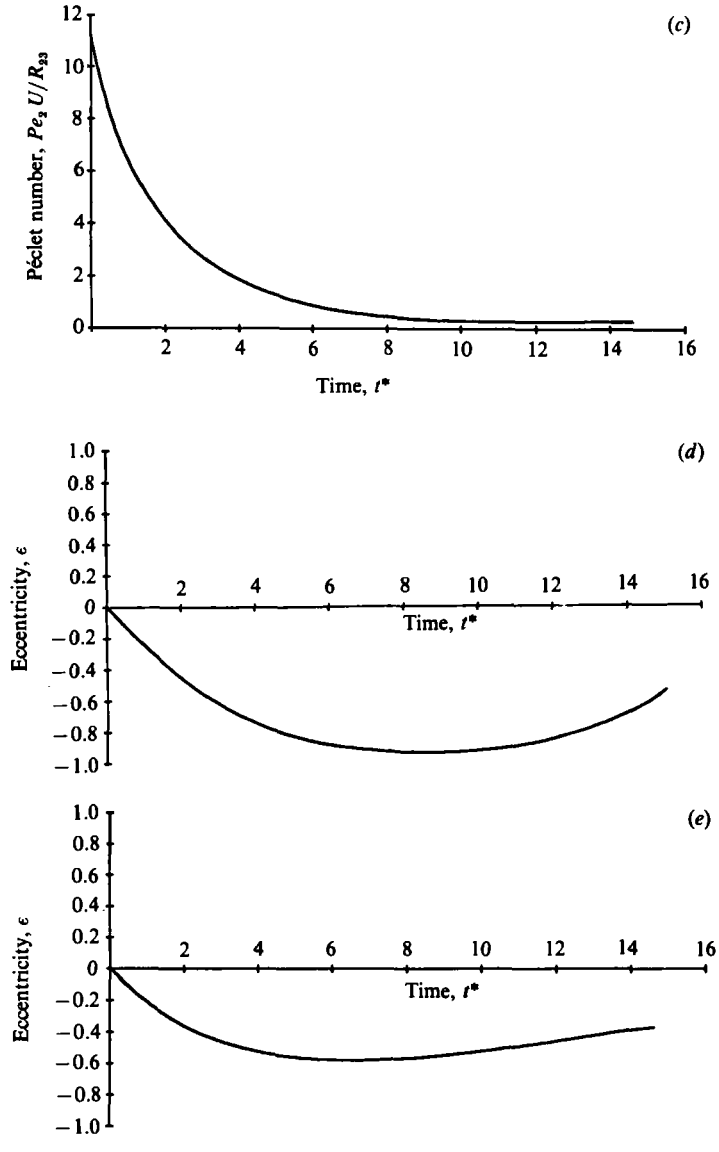

FIGURE 16. (*a*) Nusselt number as a function of time for initial $Pe_2 = 0$; (*b*) Nusselt number as a function of time for initial $Pe_2 = 40$, here Nu_c is the conduction part of the solution. (*c*) Péclet number as a function of time for case (*b*). (*d*) Eccentricity as a function of time for case (*a*) ($Pe_2 = 0$). (*e*) Eccentricity as a function of time for case (*b*) ($Pe_2 = 40$).

is given in figures 16(*d*, *e*), respectively. For both cases the eccentricity increases from zero, reaches a maximum, and then starts to decrease.

6. Conclusion

The present analysis is restricted to bubbles completely covered by their liquid phase. This situation can be a good model for the initial stages of the evaporation of a drop or the final stages of the condensation of a bubble in an immiscible fluid. The assumption of low Reynolds and capillary numbers limits the validity to small compound drops. For the case in which the continuous phase is a liquid of high

viscosity (such as castor oil at 40° C) we may allow the inner-sphere radius to be as large as 1 mm in diameter. The outer sphere could be much larger under the low-Reynolds-number approximation because the buoyant force is dominated by the size of the gaseous inner sphere. The present work helps us understand the mechanisms that control the configuration of compound drops in the case of change of phase. Numerical and fluid-mechanical limitations restricted the problem to moderate radius ratios. Eccentricity is kept within a reasonable range for computational purposes.

In the case of growth our analysis shows that, in general, the bubble is driven out of the drop owing to the buoyant forces. The viscous force generated by the radial motion tends to restore concentricity but it is not large enough to hold the bubble inside. The competing buoyant force is generally stronger in the case of growth. Also, the thinning of the liquid film around the growing bubble does not allow the film to sustain itself. As a result the vapour bubble may be left only partially surrounded by its liquid. The growth history depends very much on the initial position of the nucleating vapour bubble. The analysis for establishing the initial configuration is somewhat more involved and was not carried out in the present development.

In the case of bubble collapse, however, we see that the tendency of the bubble is to stay inside its liquid phase. This is primarily because the thinning, as in the case of growth, does not take place for collapse. Furthermore the buoyant force gets weaker as the bubble becomes smaller.

This analysis has exposed some fundamental aspects of the growth and collapse of multiphase bubbles. The time histories of the bubble dynamics tell us about the detailed behaviour of such multiphase systems and the effect of various physical parameters on important quantities such as Nusselt number and the drag force. Our future efforts will focus on other domains of multiphase drops and bubbles such as the case of a vapour bubble partially covered by its own liquid.

The authors are very grateful for the support of this research from NSF Presidential Young Investigator Award Fund (CBT 83-51432), TRW Systems, Inc. and the Ralph M. Parsons Foundation.

Appendix A

The flow field induced by a uniform stream is calculated in this Appendix. The stream functions $\psi_U^{(2)}$ and $\psi_U^{(3)}$ are given by

$$\psi_U^{(i)}(\xi,\eta) = (\cosh\xi - \cos\eta)^{-\frac{3}{2}} \sum_{n=-1}^{\infty} \Xi_n^{(i)}(\xi)\, C_{n+1}^{-\frac{1}{2}}(\cos\eta). \tag{A 1}$$

The following special forms are chosen for $\Xi^{(i)}(\xi)$:

$$\Xi_n^{(2)}(\xi) = A_n^U\left[\mathrm{e}^{(n-\frac{1}{2})(\xi-\xi_{23})} - \mathrm{e}^{(n+\frac{3}{2})(\xi-\xi_{23})}\right] + \frac{n(n+1)}{2\sqrt{2}}\left[\left(\frac{\mathrm{e}^{-(n-\frac{1}{2})\xi}}{n-\frac{1}{2}} - \frac{\mathrm{e}^{-(n+\frac{3}{2})\xi}}{n+\frac{3}{2}}\right) - \left(\frac{\mathrm{e}^{-(n-\frac{1}{2})(\xi-2\xi_{23})}}{n-\frac{1}{2}} - \frac{\mathrm{e}^{-(n+\frac{3}{2})(\xi-2\xi_{23})}}{n+\frac{3}{2}}\right)\right], \tag{A 2}$$

$$\Xi_n^{(3)}(\xi) = D_n^U\left[\frac{\sinh(n-\frac{1}{2})(\xi_{13}-\xi)}{\sinh(n-\frac{1}{2})\Delta} - \frac{\sinh(n+\frac{3}{2})(\xi_{13}-\xi)}{\sinh(n+\frac{3}{2})\Delta}\right]. \tag{A3}$$

The above forms satisfy zero-stream-function conditions at both interfaces and the zero-shear-stress condition at the inner interface. By applying the rest of the interface and boundary conditions the integration constants A_n^U and D_n^U are obtained:

$$D_n^U = \frac{A_{23}^U}{A_{23}^D}, \tag{A 4}$$

$$A_n^U = \frac{\mu_3}{\mu_2} D_n^U, \tag{A 5}$$

where

$$A_{23}^U = -\frac{n(n+1)}{\sqrt{2}}(e^{-(n-\frac{1}{2})\xi_{23}} - e^{-(n+\frac{3}{2})\xi_{23}}),$$

$$A_{23}^D = -F_n + \frac{2\mu_3}{\mu_2},$$

$$F_n = \frac{n-\frac{1}{2}}{\tanh(n-\frac{1}{2})\Delta} - \frac{n+\frac{3}{2}}{\tanh(n+\frac{3}{2})\Delta},$$

$$\Delta = \xi_{13} - \xi_{23}.$$

In terms of the above constants the drag coefficients α_2 and α_3 are given by

$$\alpha_2 = -2\sqrt{2}\sinh\xi_{23} S_{23}^U \tag{A 6}$$

and

$$\alpha_3 = -2\sqrt{2}\sinh\xi_{23} S_{13}^U \frac{\mu_3}{\mu_2}, \tag{A 7}$$

where

$$S_{23}^U = \sum_{n=1}^{\infty} 2(e^{-(n-\frac{1}{2})\xi_{23}} - e^{-(n+\frac{3}{2})\xi_{23}}) A_n^U - \frac{n(n+1)}{\sqrt{2}}\left(\frac{e^{-(n-\frac{1}{2})\xi_{23}}}{n-\frac{1}{2}} - \frac{e^{-(n+\frac{3}{2})\xi_{23}}}{n+\frac{3}{2}}\right)$$

and

$$S_{13}^U = \sum_{n=1}^{\infty} -\left(\frac{e^{-(n-\frac{1}{2})\xi_{13}}}{\sinh(n-\frac{1}{2})\Delta} - \frac{e^{-(n+\frac{3}{2})\xi_{13}}}{\sinh(n+\frac{3}{2})\Delta}\right) D_n^U.$$

Appendix B

The flow field created by the relative motion of the inner sphere is calculated here. Related stream functions $\psi_V^{(2)}$ and $\psi_V^{(3)}$ are given by

$$\psi_V^{(i)}(\xi,\eta) = (\cosh\xi - \cos\eta)^{-\frac{3}{2}} \sum_{n=-1}^{\infty} \Xi_n^{(i)}(\xi) C_{n+1}^{-\frac{1}{2}}(\cos\eta). \tag{B 1}$$

The following special forms are selected for this case:

$$\Xi_n^{(2)}(\xi) = A_n^V[e^{(n-\frac{1}{2})(\xi-\xi_{23})} - e^{(n+\frac{3}{2})(\xi-\xi_{23})}], \tag{B 2}$$

$$\Xi_n^{(3)}(\xi) = C_n^V\left[\frac{\sinh(n-\frac{1}{2})(\xi-\xi_{23})}{\sinh(n-\frac{1}{2})\Delta} - \frac{\sinh(n+\frac{3}{2})(\xi-\xi_{23})}{\sinh(n+\frac{3}{2})\Delta}\right]$$
$$+ D_n^V\left[\frac{\sinh(n-\frac{1}{2})(\xi_{13}-\xi)}{\sinh(n-\frac{1}{2})\Delta} - \frac{\sinh(n+\frac{3}{2})(\xi_{13}-\xi)}{\sinh(n+\frac{3}{2})\Delta}\right] + E_n^V \frac{\sinh(n-\frac{1}{2})(\xi-\xi_{23})}{\sinh(n-\frac{1}{2})\Delta}, \tag{B 3}$$

so that zero stream function at the outer interface is satisfied. The integration constants are given by

$$E_n^V = \frac{n(n+1)}{2\sqrt{2}}\left[\frac{e^{-(n-\frac{1}{2})\xi_{13}}}{n-\frac{1}{2}} - \frac{e^{-(n+\frac{3}{2})\xi_{13}}}{n+\frac{3}{2}}\right], \tag{B 4}$$

$$C_n^V = \tfrac{1}{2}[(n-\tfrac{1}{2})E_n^V + \tau_{13}^V], \tag{B 5}$$

and

$$D_n^V = \frac{A_{23}^V}{A_{23}^D}, \tag{B 6}$$

$$A_n^V = \frac{\mu_3}{\mu_2} D_n^V, \tag{B 7}$$

where

$$\tau_{13}^V = -\frac{n(n+1)}{\sqrt{2}} \mathrm{e}^{-(n+\frac{1}{2})\xi_{13}} \sinh \xi_{13},$$

$$A_{23}^V = -\frac{n-\frac{1}{2}}{\sinh (n-\frac{1}{2})\Delta} E_n^V - G_n C_n^V$$

and

$$G_n = \frac{n-\frac{1}{2}}{\sinh (n-\frac{1}{2})\Delta} - \frac{n+\frac{3}{2}}{\sinh (n+\frac{3}{2})\Delta}$$

The drag coefficients β_2 and β_3 are then given by

$$\beta_2 = -2\sqrt{2} \sinh \xi_{23} S_{23}^V \tag{B 8}$$

and

$$\beta_3 = -2\sqrt{2} \sinh \xi_{23} S_{13}^V \frac{\mu_3}{\mu_2}, \tag{B 9}$$

where

$$S_{23}^V = \sum_{n=1}^{\infty} 2(\mathrm{e}^{-(n-\frac{1}{2})\xi_{23}} - \mathrm{e}^{-(n+\frac{3}{2})\xi_{23}}) A_n^V$$

and

$$S_{13}^V = \sum_{n=1}^{\infty} \left(\frac{\mathrm{e}^{-(n-\frac{1}{2})\xi_{23}}}{\sinh (n-\frac{1}{2})\Delta} - \frac{\mathrm{e}^{-(n+\frac{3}{2})\xi_{23}}}{\sinh (n+\frac{3}{2})\Delta} \right) C_n^V$$
$$- \left(\frac{\mathrm{e}^{-(n-\frac{1}{2})\xi_{13}}}{\sinh (n-\frac{1}{2})\Delta} - \frac{\mathrm{e}^{-(n+\frac{3}{2})\xi_{13}}}{\sinh (n+\frac{3}{2})\Delta} \right) D_n^V + \frac{\mathrm{e}^{-(n-\frac{1}{2})\xi_{23}}}{\sinh (n-\frac{1}{2})\Delta} E_n^V.$$

Appendix C

The integration constants of the stream functions $\psi_{V_r}^{(i)}$ are A_n, B_n, C_n, D_n and E_n. We give B_n and E_n in the main text following (49). The rest of the constants are

$$C_n = \tfrac{1}{2}[(n-\tfrac{1}{2})E_n + \tau_{13}], \tag{C 1}$$

$$D_n = \frac{A_{23}}{A_{23}^D}, \tag{C 2}$$

$$A_n = \frac{\mu_3}{\mu_2} D_n - \frac{1}{2}\left(\frac{\mu_3}{\mu_2} - 1\right)(\tau_{23} + (n-\tfrac{1}{2})B_n), \tag{C 3}$$

where

$$\tau_{13} = -\frac{3}{2\sqrt{2}}\left[\frac{(n+\frac{3}{2})\mathrm{e}^{-(n-\frac{1}{2})\xi_{13}} - (n-\frac{1}{2})\mathrm{e}^{-(n+\frac{3}{2})\xi_{13}}}{\sinh \xi_{13}} - \mathrm{e}^{-(n+\frac{1}{2})\xi_{13}} \sinh \xi_{13} A' \right],$$

$$\tau_{23} = -\frac{3}{2\sqrt{2}}\left[\frac{((n+\frac{3}{2})\mathrm{e}^{-(n-\frac{1}{2})\xi_{23}} - (n-\frac{1}{2})\mathrm{e}^{-(n+\frac{3}{2})\xi_{23}})R^2}{\sinh \xi_{23}} - \mathrm{e}^{-(n+\frac{1}{2})\xi_{23}} \sinh \xi_{23} B' \right],$$

and

$$A_{23} = -\left(\frac{n-\frac{1}{2}}{\sinh (n-\frac{1}{2})\Delta} E_n - \frac{n-\frac{1}{2}}{\tanh (n-\frac{1}{2})\Delta} B_n - G_n C_n \right) + \left(\frac{\mu_3}{\mu_2} - 1 \right)\tau_{23} + \frac{\mu_3}{\mu_2}(n-\tfrac{1}{2})B_n.$$

The drag coefficients γ_2 and γ_3 are given as

$$\gamma_2 = -2\sqrt{2}\sinh\xi_{23} S_{23}^{V_r} \tag{C 4}$$

and

$$\gamma_3 = -2\sqrt{2}\sinh\xi_{23} S_{13}^{V_r}\frac{\mu_3}{\mu_2}, \tag{C 5}$$

where $$S_{23}^{V_r} = 8A^{*(2)} + \sum_{n=1}^{\infty} 2(\mathrm{e}^{-(n-\frac{1}{2})\xi_{23}} - \mathrm{e}^{-(n+\frac{3}{2})\xi_{23}})A_n + 2\mathrm{e}^{-(n-\frac{1}{2})\xi_{23}}B_n$$

and

$$S_{13}^{V_r} = 8A^{*(3)} + \sum_{n=1}^{\infty}\left(\frac{\mathrm{e}^{-(n-\frac{1}{2})\xi_{23}}}{\sinh(n-\frac{1}{2})\Delta} - \frac{\mathrm{e}^{-(n+\frac{3}{2})\xi_{23}}}{\sinh(n+\frac{3}{2})\Delta}\right)C_n + \frac{\mathrm{e}^{-(n-\frac{1}{2})\xi_{23}}}{\sinh(n-\frac{1}{2})\Delta}E_n$$
$$-\left(\frac{\mathrm{e}^{-(n-\frac{1}{2})\xi_{13}}}{\sinh(n-\frac{1}{2})\Delta} - \frac{\mathrm{e}^{-(n+\frac{3}{2})\xi_{13}}}{\sinh(n+\frac{3}{2})\Delta}\right)D_n - \frac{\mathrm{e}^{-(n-\frac{1}{2})\xi_{13}}}{\sinh(n-\frac{1}{2})\Delta}B_n$$

REFERENCES

GOREN, S. L. & O'NEILL, M. E. 1971 On the hydrodynamic resistance to a particle of a dilute suspension when in the neighborhood of a large obstacle. *Chem. Engng Sci.* **26**, 325–338.

HABER, S., HETSRONI, G. & SOLAN, A. 1973 On the low Reynolds number motion of two droplets. *Intl J. Multiphase Flow* **1**, 57–71.

HAYAKAWA, T. & SHIGETA, M. 1974 Terminal velocity of two-phase droplet. *J. Chem. Engng Japan* **7**, 140–142.

ISENBERG, J. & SIDEMAN, S. 1970 Direct contact heat transfer with change of phase: bubble condensation in immiscible liquids. *Int J. Heat Mass Transfer* **13**, 997–1011.

JACOBS, H. R. & MAJOR, B. H. 1982 The effect of noncondensible gases on bubble condensation in an immiscible liquid. *Trans. ASME* C: *J. Heat Transfer* **104**, 487–492.

JEFFERY, G. B. 1912 On a form of the solution of Laplace's equation suitable for problems relating two spheres. *Proc. R. Soc. Lond.* A **87**, 115.

JOHNSON, R. E. & SADHAL, S. S. 1985 Fluid mechanics of compound multiphase drops and bubbles. *Ann. Rev. Fluid Mech.* **17**, 289–320.

LERNER, Y. & LETAN, R. 1985 Dynamics of condensing bubbles: effects of injection frequency. *22nd National Heat Transfer Conference, Denver, Colorado, August 4–7, 1985, paper no.* 85-HT-47.

MEYYAPAN, M., WILCOX, W. R. & SUBRAMANIAN, R. S. 1981 Thermocapillary migration of a bubble normal to a plane surface. *J. Colloid Interface Sci.* **83**, 199–208.

O'NEILL, M. E. 1964 A slow motion of a viscous fluid caused by a slowly moving solid sphere. *Mathematica* **11**, 67–74.

PLESSET, M. S. & PROSPERETTI, A. 1977 Bubble dynamics and cavitation. *Ann. Rev. Fluid Mech.* **9**, 145–185.

PROSPERETTI, A. & PLESSET, M. S. 1978 Vapour-bubble growth in a superheated liquid. *J. Fluid Mech.* **85**, 349–368.

RASMUSSEN, R. M., LEVIZZANI, V. R. & PRUPPACHER, H. R. 1982 A numerical study of heat transfer through a fluid layer with recirculating flow between concentric and eccentric spheres. *Pure Appl. Geophys.* **120**, 702–720.

RUSHTON, E. & DAVIES, G. A. 1973 The slow unsteady settling of two fluid spheres along their line of centers. *Intl J. Multiphase Flow* **4**, 357–381.

RUSHTON, E. & DAVIES, G. A. 1978 The slow motion of two spherical particles along their line of centers. *Intl J. Multiphase Flow* **9**, 337–342.

SADHAL, S. S. & OĞUZ, H. N. 1985 Stokes flow past compound multiphase drops: the case of completely engulfed drops/bubbles. *J. Fluid Mech.* **160**, 511–529.

SELECKI, A. & GRADON, L. 1976 Equation of motion of an expanding vapour drop in an immiscible liquid medium. *Intl J. Heat Mass Transfer* **19**, 51–59.

SIDEMAN, S. & HIRSCH, G. **1965** Direct contact heat transfer with change of phase: condensation of single vapour bubbles in an immiscible liquid medium. Preliminary studies. *AIChE J.* **11**, 1019–1025.

SIDEMAN, S. & TAITEL, Y. **1964** Direct contact heat transfer with change of phase: evaporation of drops in an immiscible liquid medium. *Intl J. Heat Mass Transfer* **7**, 1273–1289.

STIMSON, M. & JEFFERY, G. B. **1926** The motion of two spheres in a viscous fluid. *Proc. R. Soc. Lond.* A **111**, 110–116.

STOKES, G. G. **1851** On the effect of the internal friction of fluid on the motion of pendulums. *Trans. Camb. Phil. Soc.* **9**, 8–106.

TOCHITANI, Y., MORI, Y. H. & KOMOTORI, K. **1977***a* Vaporization of single drops in an immiscible liquid. Part I. Forms and motions of vaporizing drops. *Wärme Stoffübertrag.* **10**, 51–59.

TOCHITANI, Y., NAKAGAWA, T., MORI, Y. H. & KOMOTORI, K. **1977***b* Vaporization of single liquid drops in an immiscible liquid. Part II. Heat transfer characteristics. *Wärme Stoffübertrag.* **10** 71–79.